# CHAPTER 3

# DIFFERENT REGENERATIVE EVAPORATIVE COOLING TOPOLOGIES

## 3.1. Introduction

The fluid flow directions have a significant impact on the heat and mass exchanger's performance. In general, the heat and mass exchanger (HMX) of regenerative evaporative coolers may be parallel/counter flow or cross flow type. Several configurations are possible for both parallel/counter and cross-flow regenerative evaporative coolers. So there is a need to do a comparative analysis of all the possible configurations of a regenerative evaporative cooler. Furthermore, the energy, exergy, economic and environmental analyses are very important tools for this comparison. In the present investigation, a total of eight possible configurations (four each for counter/parallel and cross flows) of the regenerative evaporative cooler are evaluated by taking water flow in gravitational direction, and the effect of important operating and design parameters on the performance is studied. Fig. 3.1 contains all configurations of counter/parallel flow, while Fig. 3.2 contains all configurations of the cross-flow regenerative evaporative cooler. In configurations A and C, primary and secondary air is in the counter flow direction, while in configurations B and D, they are in the parallel flow direction. Secondary airflow direction is aligned with the water flow direction in configuration A, and D. The primary air and secondary air is in cross flow for the configuration E, F, G, and H. Secondary air flow parallel to the water flow direction, for configuration E while in counter flow direction for configuration F. Primary air flows

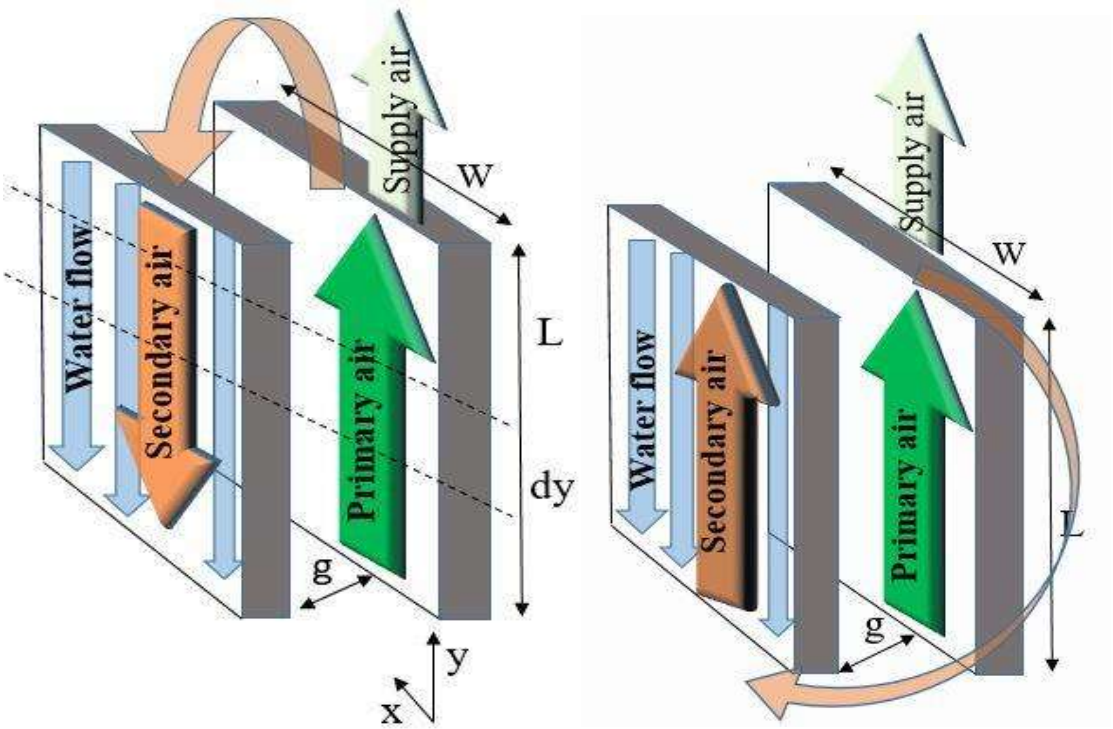


(a) Configuration-A (b) Configuration-B

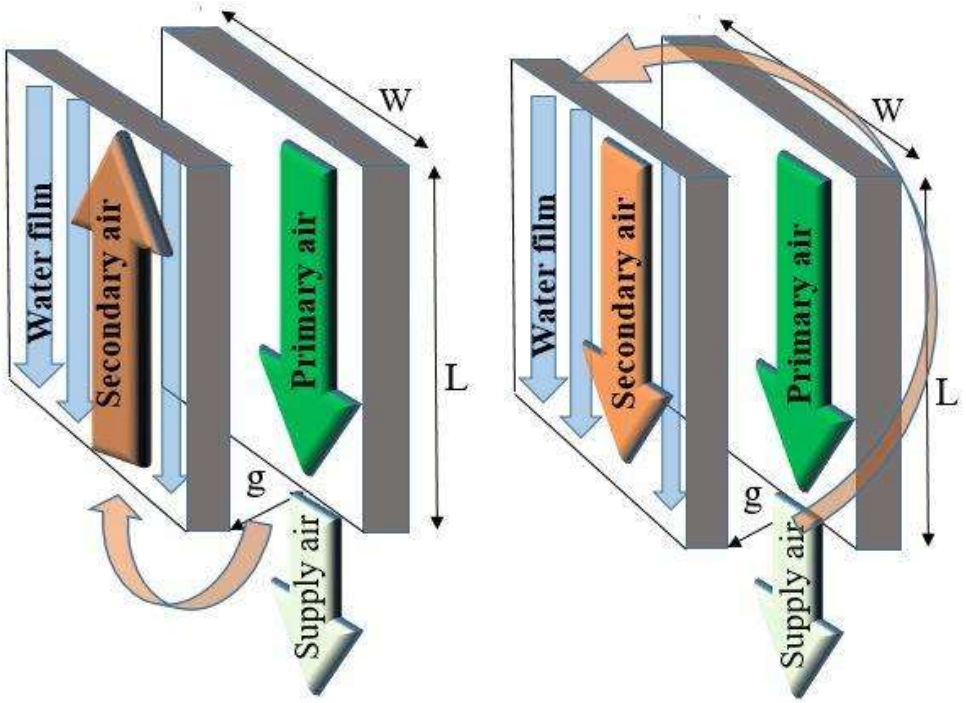


(c) Configuration-C (d) Configuration –D

**Fig. 3.1** Four configurations of regenerative parallel/counter flow evaporative cooler

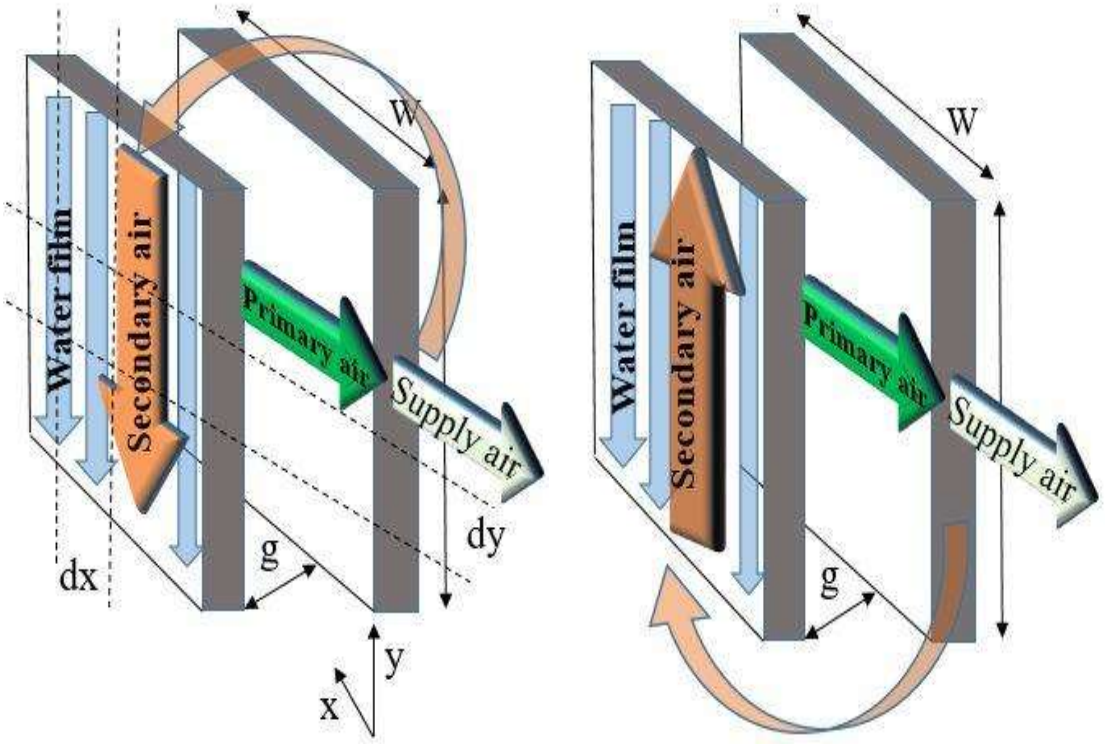


(a) Configuration-E (b) Configuration -F

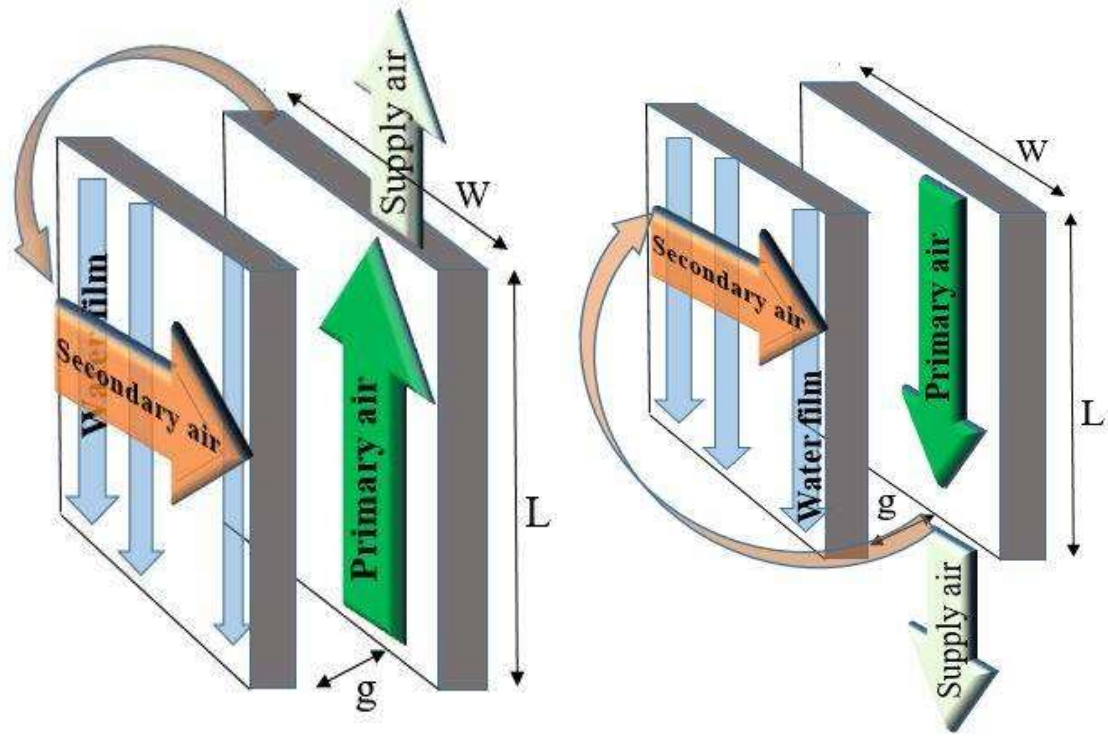


(c) Configuration-G (d) Configuration-H

**Fig. 3.2** Four configurations of the regenerative cross-flow evaporative cooler

counter to the water flow direction, for configuration G while in parallel flow direction for configuration F.

### 3.2 Numerical model and simulation

The differential element of configuration A and configuration E of regenerative evaporative heat and mass exchanger (HMX) is shown in Fig. 3.3. The governing equations are the energy and mass conservation equations in the channels of the regenerative evaporative cooler. Some assumptions are made to simplify the mathematical modeling for all configurations, which are mentioned below.

(i) The whole evaporative heat and mass exchanger is assumed well insulated (there is no exchange of heat in between surrounding and air inside). (These assumptions neglect the little amount of heat exchange with the outer plate and side casing of the HMX, hence little over predict the performance.)

(ii) The heat and mass exchange processes inside the exchanger are assumed to be steady and fully developed. (The flow developing length is very small as compared to the fully developed length; hence it have a negligible effect on the result.)

(iii) The gap between the channels is very small in comparison to the width of the device; hence, the numerical model is treated as one-dimensional.

(iv) The air-flow inside the evaporative cooler is laminar. (The very narrow airflow gap results in a small characteristic dimension of fluid flow. That's why there is low Reynold number flow inside the channels.)

(v) The coefficients of mass transfer and heat transfer are assumed to be constant for the whole channel length. (Since this is a low-temperature difference application hence there are no significant variations in the values.)

(vi) The air just above the water film surface is considered to be fully saturated at water temperature in that discrete element. (The mass transfer takes place due to a

concentration gradient, and it helps to obtain water vapour concentration at the surface.)

(vii) The whole surface is assumed to be uniformly wet and covered by a water film. (The Kraft paper has been assumed as a wetting material on the wet surface of the regenerative evaporative cooler, which has good surface wetting characteristics.The whole surface is assumed to be uniformly wet and covered by a water film. Hence, the surface wettability factor has been assumed closer to 1.)

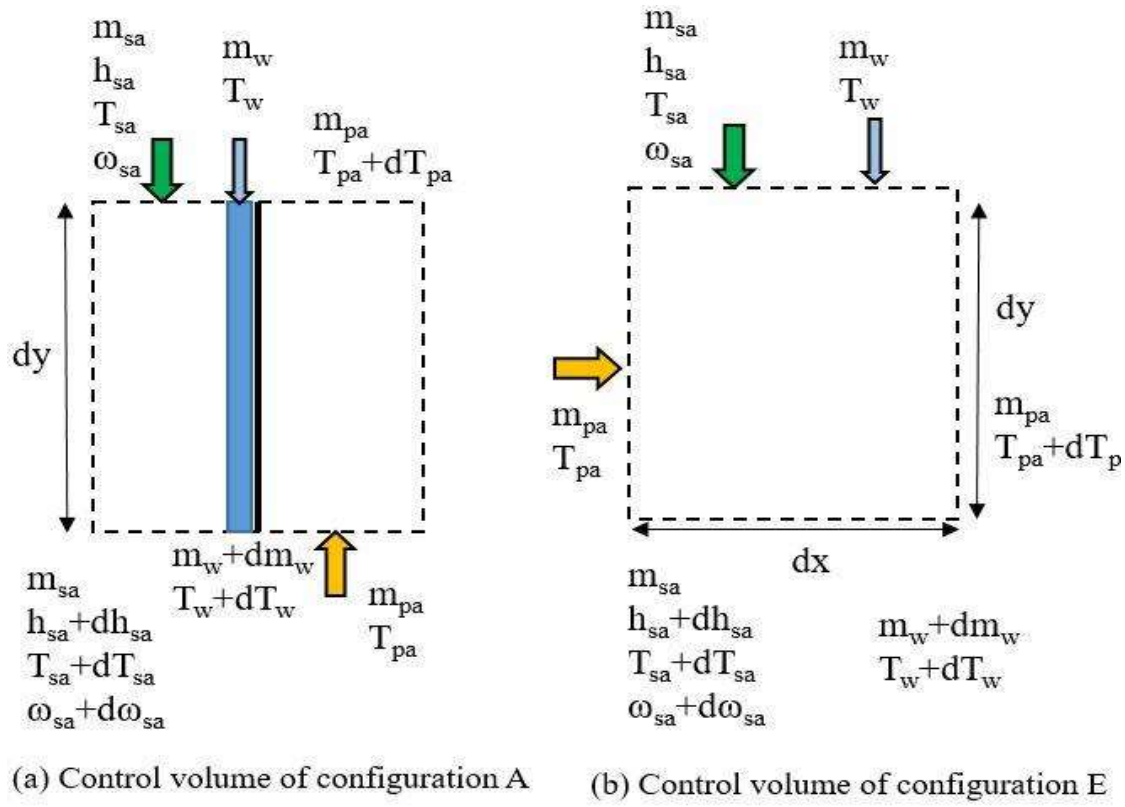


**Fig. 3.3.** Control volume of evaporative heat and mass exchanger

The kraft paper is conventionally used as a wetting material on the wet surface of the heat exchanger, which shows good surface wetting characteristics. Xu et al. (2016) compared different fabrics and found some fabrics show 171 to182% higher wicking ability, which makes the surface wettability factor of the fabric closer to 1 depending upon the good distribution system of the water. The fabric should be glued on the surface, as recommended by Duan. (2011). Water should be supplied at more than one height,

depending upon the wicking height of the fabric. As recommended by Gao et al. (2015), the water flow rate needs to be five times greater than the water evaporation rate. Lee et al. (2013) experimentally showed that the higher effectiveness of the device is obtained if supplied to the water evaporated ratio is around five and lesser. Hence, based on the recommendations of the above experimental studies, good surface wetting behavior and good water distribution are assumed, and the water flow rate is always taken greater than five times of evaporation rate to justify the last assumption.

### *3.2.1 Mathematical model*

Based on the above assumptions, the governing equations are written in general form, applicable to all configurations. The primary air in the dry channel transfers heat to the flowing water film on the wet side through convective heat transfer in the primary air, thermal conduction through the plate and convective heat transfer in the water film. Energy conservation for the primary air gives,

$$\dot{m}_{pa} c_{p,pa} dT_{pa} = U(T_w - T_{pa})dA \tag{3.1}$$

The inverse of overall heat transfer coefficient includes all resistance between the primary air and flowing water. This includes primary air side and water side convection coefficients, and conduction in the plate. Where U is obtained by, $\frac{1}{U} = \frac{1}{\alpha_{pa}} + \frac{t_{plate}}{k_{plate}} + \frac{1}{\alpha_w}$

The convection and evaporation (latent) heat transfer takes place between the secondary air and water film. The energy conservation of the secondary air yields,

$$\dot{m}_{sa} dh_{sa} = [\alpha_{sa}(T_w - T_{sa}) + h_{wv}\kappa_m(\omega_{ws} - \omega_{sa})]dA \tag{3.2}$$

Where water vapor specific enthalpy at a temperature of water film is given by,

$$h_{wv} = h_{fg} + c_{p,v} T_w \tag{3.3}$$

And specific enthalpy of secondary air is given by,

$$h_{sa} = c_{p,sa} T_{sa} + \omega_{sa} h_{fg} \tag{3.4}$$

The mass conservations in the secondary air channel for a differential control volume is

$$\dot{m}_{sa} d\omega_{sa} = \kappa_m (\omega_{ws} - \omega_{sa}) dA \tag{3.5}$$

Where $\omega_{ws}$ is saturated air humidity at water film temperature, and $\omega_{sa}$ is the humidity of secondary air.

The overall energy balance for the control volume includes the primary air, secondary air and water film energy conservation and for the differential element is expressed as,

$$\dot{m}_{pa} c_{p,pa} dT_{pa} + \dot{m}_{sa} dh_{sa} + \dot{m}_w c_{p,w} dT_w + c_{p,w} T_w d\dot{m}_w = 0 \tag{3.6}$$

Where $d\dot{m}_w = \dot{m}_{sa} d\omega_{sa}$. The air-stream flow inside the evaporative HMX is laminar due to the lower flow velocity and small hydraulic diameter. The correlation used to calculate the Nusselt number for flow inside the primary and secondary air channels is given by (Zhan et al., 2011),

$$Nu = 2 + 0.6 Re^{0.5} Pr^{0.33} \tag{3.7}$$

Where, $Re = \frac{\rho_{pa} d_h u_{pa}}{\mu_{pa}}$ (for primary air) and $Re = \frac{\rho_{sa} d_h u_{ra}}{\mu_{sa}}$ (for secondary air).

To consider the relative effect, of air velocity and water velocity, relative air velocity ($u_{ra}$) has been used in the wet channel. The relative air velocity in the wet channel for different configurations is mentioned in Table 3.1. The Nu correlation is applied for both cross-flow (Moshari et al., 2015) as well as parallel/counter-flow (Liu et al., 2019, Cui et al., 2014) configurations. The heat transfer coefficient in primary and secondary air channels has been calculated by respectively,

$$\alpha_{pa} = Nu\left(k_{pa} / d_{h,pa}\right) \tag{3.8}$$

$$\alpha_{sa} = Nu\left(k_{sa} / d_{h,sa}\right) \tag{3.9}$$

For air flowing in both dry and wet channels, $d_h = 2g$.

The Nusselt number correlation used for downward flowing water film is Nu = 1.88 (Liu et al., 2019), and hence the heat transfer coefficient of the water film is determined as,

$$\alpha_w = Nu_w \left( k_w / \delta_w \right) \tag{3.10}$$

Where, $\delta_w = \dfrac{3\nu_w \Gamma}{\rho_w g}$ and $\Gamma = \dfrac{m_w}{(n+1)W}$

The mass transfer coefficient is calculated as $\kappa_m = \alpha_{sa} / (c_{p,sa} Le)$ (3.11)

Where Le is the Lewis factor. The Lewis factor of the air-water mixture is $(0.87)^{2/3}$ at standard atmospheric conditions.

The boundary conditions for all eight configurations are listed in Table 3.1. The y = 0 represents the bottom surface, and y = L represents the top surface of the heat and mass exchanger. In the cross-flow configurations, x = 0 represents the left surface while x = W represents the rightmost surface of the heat and mass exchanger.

**Table 3.1**: Boundary condition for all eight configurations of HMX

| Configuration A | Configuration B |
|---|---|
| $T_{pa}$ (y = 0) = $T_{in}$ | $T_{pa}$ (y = 0) = $T_{in}$ |
| $T_{sa}$ (y = L) = $T_{pa}$ (y = L) | $T_{sa}$ (y = 0) = $T_{pa}$ (y = L) |
| $\omega_{sa}$ (y = L) = $\omega_{in}$ | $\omega_{sa}$ (y = 0) = $\omega_{in}$ |
| $T_w$ (y = L) = $T_{w,in}$ | $T_w$ (y = L) = $T_{w,in}$ |
| $u_{ra} = u_{sa} - u_w$ | $u_{ra} = u_{sa} + u_w$ |
| **Configuration C** | **Configuration D** |
| $T_{pa}$ (y = L) = $T_{in}$ | $T_{pa}$ (y = L) = $T_{in}$ |
| $T_{sa}$ (y = 0) = $T_{pa}$ (y = 0) | $T_{sa}$ (y = L) = $T_{pa}$ (y = 0) |
| $\omega_{sa}$ (y = 0) = $\omega_{in}$ | $\omega_{sa}$ (y = L) = $\omega_{in}$ |
| $T_w$ (y = L) = $T_{w,in}$ | $T_w$ (y = L) = $T_{w,in}$ |
| $u_{ra} = u_{sa} + u_w$ | $u_{ra} = u_{sa} - u_w$ |

| Configuration E | Configuration F |
|---|---|
| $T_{pa}\ (x = 0) = T_{in}$<br>$T_{sa}\ (y = L) = T_{pa}\ (x = W)$<br>$\omega_{sa}\ (y = L) = \omega_{in}$<br>$T_{w}\ (y = L) = T_{w,in}$<br>$u_{ra} = u_{sa} - u_{w}$ | $T_{pa}\ (x = 0) = T_{in}$<br>$T_{sa}\ (y = 0) = T_{pa}\ (x = W)$<br>$\omega_{sa}\ (y = 0) = \omega_{in}$<br>$T_{w}\ (y = L) = T_{w,in}$<br>$u_{ra} = u_{sa} + u_{w}$ |
| **Configuration G** | **Configuration H** |
| $T_{pa}\ (y = L) = T_{in}$<br>$T_{sa}\ (x = 0) = T_{pa}\ (y = 0)$<br>$\omega_{sa}\ (x = 0) = \omega_{in}$<br>$T_{w}\ (y = L) = T_{w,in}$<br>$u_{ra} = u_{sa}$ | $T_{pa}\ (y = 0) = T_{in}$<br>$T_{sa}\ (x = 0) = T_{pa}\ (y = L)$<br>$\omega_{sa}\ (x = 0) = \omega_{in}$<br>$T_{w}\ (y = L) = T_{w,in}$<br>$u_{ra} = u_{sa}$ |

### *3.2.2 Numerical method and performance parameters*

The Coupled differential equations are discretized with the finite difference method. Discretised differential equations are solved in Engineering Equation Solver (EES) (Klein, 2017**).** Inbuilt functions of EES are used to calculate the properties of humid air, water, and water vapor. EES solves the system of equations by an iteration using Newtons method. The performances of the evaporative cooler are evaluated by cooling capacity, effectiveness, and coefficient of performance (COP).

As the primary air humidity remains the same in the regenerative evaporative cooler, the effectiveness represents the ratio of actual temperature drop to the maximum possible temperature drop, which is up to the dew point. Hence, this effectiveness, which is called dew-point effectiveness (DPE), is determined by,

$$\varepsilon = \frac{T_{pa,in} - T_{pa,out}}{T_{pa,in} - T_{pa,dew-point}} \tag{3.12}$$

The cooling capacity of cooler (heat removal rate from cooling space) is given as,

$$Q_{system} = \dot{m}_{out} c_{p,pa} (T_{pa,in} - T_{pa,out}) \tag{3.13}$$

The total pressure drop in HMX channels consists of pressure loss in the primary air (dry air) channel and pressure loss in the secondary air (wet air) channel. Again the pressure drop of air in the channels consists of both frictional losses (major losses) and local (minor) losses. The pressure drop of primary air consists of contraction, frictional, straight-line flow, and outlet air filter losses, and hence given by (Duan et al., 2017),

$$\Delta p_{pa} = f \frac{\rho_{pa} u_{pa}^2}{2 d_h} L + \sum \zeta \frac{\rho_{pa} u_{pa}^2}{2} \tag{3.14}$$

The average friction factor (Duan et al., 2017),

$$f = \frac{4}{\mathrm{Re}} \left[ \frac{3.44}{\sqrt{l^+}} + \frac{\frac{1.25}{4l^+} + \frac{f_{fd}\,\mathrm{Re}}{4} - \frac{3.44}{\sqrt{l^+}}}{1 + \frac{0.00021}{(l^+)^2}} \right] \tag{3.15}$$

where $l^+ = \frac{L}{d_h \,\mathrm{Re}}$ and $f_{fd} = \frac{96}{\mathrm{Re}}$ (Incropera et al., 2017), which is friction factor for fully developed flow . The resistance coefficient ζ sums up the coefficient for sudden inlet contraction, flow in the tee straight (loss coefficient 0.1), and resistance of air flowing through the air filter.

The pressure drop of the secondary air channel consists of frictional loss, tee branch flow loss, sudden contraction, sudden expansion, bend loss, and exit loss in the secondary air channel (relative velocity is considered for this frictional loss) and sudden outlet expansion-

$$\Delta p_{sa} = f\frac{\rho_{sa}u_{sa}^2}{2d_h}L + (\zeta_{tee,branched} + \zeta_{contraction} + \zeta_{expansion} + \zeta_{bend} + \zeta_{exit})\frac{\rho_{sa}u_{sa}^2}{2} \quad (3.16)$$

The value of the loss coefficient is 0.9, 0.5, 1, 1.5, and 1 for tee branching, contraction, expansion, bend, and exit of the channel, respectively. The actual fan power is given by,

$$P_{fan} = \frac{\Delta p_{pa}V_{pa} + (\varsigma_{exit} + \varsigma_{filter})\frac{\rho u^2_{supply}}{2}(V_{pa} - V_{sa}) + \Delta p_{sa}V_{sa}}{\eta_{fan}} \quad (3.17)$$

Where $\eta_{fan}$ is taken as 0.65 (Duan et al., 2017), and air filter pressure drop coefficients are calculated by ventilation Components pressure drop data (Engineering ToolBox, 2003). The resistance coefficient value for exit air and air filer, respectively.

Theoretical pump power = $\dot{m}_w g H_{total}$ ; where g is the acceleration due to gravity and $H_{total}$ = $H_{valve}$ + $H_{gravity}$ + $H_{frictional}$ + $H_{nozzle}$. $H_{valve}$ = 1.5 m, $H_{gravity}$= 3 m, $H_{nozzle}$= 1.5 m and $H_{frictional} = \frac{64}{\mathrm{Re}_w}\frac{L_{pipe}}{d_{pipe}}\frac{V_w^2}{2g}$. Where $L_{pipe}$ is the length of pipe and $d_{pipe}$ is the diameter of the pipe used to circulate water.

Actual pump power ($P_{pump}$) = theoretical pump power/$\acute{\eta}_{pump}$. Pump efficiency ($\acute{\eta}_{pump}$) is around 60% in this study.

Coefficient of performance is given by,

$$\mathrm{COP} = Q_{system} / (P_{fan} + P_{pump}) \quad (3.18)$$

### *3.2.3 Exergy analysis*

Total flow exergy of the humid air per kg of dry air is expressed as (Chengqin et al., 2002)

$$\psi_{Total} = \psi_{chemical} + \psi_{mechanical} + \psi_{thermal} \quad (3.19)$$

$$\psi_{thermal} = (c_p + \omega c_{p,v})T_0\left(\frac{T}{T_0} - 1 - \ln\frac{T}{T_0}\right) \quad (3.20)$$

$$\psi_{mechanical} = (1+1.608\omega) R_a T_0 \ln \frac{p}{p_0} \quad (3.21)$$

$$\psi_{chemical} = R_a T_0 \{(1+1.608\omega) \ln \frac{1+1.608\omega_0}{1+1.608\omega} + 1.608\omega \ln \frac{\omega}{\omega_0}\} \quad (3.22)$$

Where $T_0$, $p_0$, $\omega_0$ are the temperature, pressure, and humidity at the reference state. $R_a$ is the dry air-specific gas constant. This total exergy is separated into thermal exergy, mechanical exergy, and chemical exergy. Exergy balance is given by (Farmahini-Farahani et al., 2012),

$$\dot{E}x_{pa} + \Delta\dot{E}x_w - \dot{E}x_{supply\text{-}air} - \dot{E}x_{sa} - \dot{I} = 0 \quad (3.23)$$

Where, $\dot{E}x_{pa} = \dot{m}_{pa}\psi_{pa}$ , $\Delta\dot{E}x_w = \Delta\dot{m}_w\psi_w$ , $\dot{E}x_{supply\text{-}air} = \dot{m}_{supply\text{-}air}\psi_{supply\text{-}air}$

$\dot{E}x_{sa} = \dot{m}_{sa}\psi_{sa}$ and $\dot{I}$ is exergy destruction.

Here, $\Delta\dot{m}_w = \dot{m}_{sa}(\omega_{sa\text{-}in} - \omega_{sa\text{-}out})$ and $\psi_w = -R_v T_0 \ln\varphi_0$

$R_v$ is the water vapor-specific gas constant, and $\varphi_0$ is the relative humidity at the reference state. The atmospheric saturation state is considered the reference state.

$$\eta_{ex} = \frac{\dot{E}x_{supplyair\text{-}out} - \dot{E}x_{supplyair\text{-}in}}{\dot{E}x_{sa\text{-}in} + \dot{E}x_w - \dot{E}x_{sa\text{-}out}} \quad (3.24)$$

### *3.2.4 Economic analysis*

The total cost is the sum of the operating cost and the capital cost (initial cost) of the device. The main components of the device are a fan, pump, and heat, and mass exchanger (HMX). The total capital cost of the device is:

$$C_{Capital\ cost} = C_{Axial\ fan} + C_{Tangential\ fan} + C_{Water\ pump} + C_{HMX} + C_{casing} + C_{tank} + C_{Water\ piping} \quad (3.25)$$

Where C denotes the cost. The Capital cost of the components is calculated by expressions (Sohani et al., 2018) listed in Table 3.2. The total cost is:

$$C_{Total\ cost} = C_{Capital\ cost} + C_{Operating\ cost} + C_{Maintenance\ cost} \quad (3.26)$$

The maintenance cost varied from 1% to 5% of the initial capital cost of the evaporative cooler. In this analysis, it is considered to be 5% (Sohani et al., 2018).

**Table 3.2**: The component capital cost of the HMX

| Components | unit | Cost (USD) |
|---|---|---|
| Axial fan | 1 | $68.51\left(\frac{Power_{fan}}{70}\right)^{0.6}$ |
| Tangential fan | 1 | $90.29\left(\frac{Power_{fan}}{72}\right)^{0.6}$ |
| Water pump | 1 | $5.1\left(\frac{m_{airflow}}{1500}\right)^{0.6}$ |
| Heat and mass exchanger (HMX) | 1 | $112\left(\frac{A_{plate}}{100.24}\right)^{0.6}$ |
| Casing | 1 | $156\left(\frac{A_{casing}}{4.26}\right)^{0.6}$ |
| Upper tank | 1 | $7.5\left(\frac{Volume_{tank}}{21}\right)^{0.6}$ |
| Lower tank | 1 | $8.5\left(\frac{Volume_{tank}}{21}\right)^{0.6}$ |
| Water piping | 1 | $13\left(\frac{Volume_{cooler}}{0.50}\right)^{0.6}$ |

The operating cost (running cost) of the cooler is obtained by the power consumption of the fan and water pump. It is assumed that HMX is operating eight working hours in a day and 180 working days over a period of one year. The specific total cost is defined as the cost per unit cooling capacity of the device.

Specific total cost (STC) = $\frac{C_{Total\,cost}}{Q_{system}}$ (3.27)

The net present value (NPV) represents the present worth of the all-cash flows in the future and is calculated as (Bellos et al.,2017) $NPV = -C_{capitalcost} + \sum_{j=1}^{M} \frac{Cf_{net}}{(1+r)^j}$ (3.28)

The net cash flow ( $Cf_{net}$ ) is the summation of the cooling production cost, operation and maintenance cost, and electrical consumption cost. It is calculated as

$$Cf_{net} = C_{ref} Y_e - C_{o\&m} C_{capitalcost} - C_{el} Y_{el} \quad (3.29)$$

The $Y_e$ is the yearly cooling production, and $Y_{el}$ is the yearly electrical consumption, which is calculated for the six months/year and 8 hours/day of device running duration. The cost of refrigeration is calculated as $C_{ref} = \frac{C_{el}}{COP_{eq}}$ , where $C_{el}$ is the electrical consumption cost. The $COP_{eq}$ is the coefficient of performance of the equivalent (same cooling capacity) vapor compression system. The internal rate of return (IRR) is a very important economic parameter of any investment. IRR can be calculated as

$$IRR = \frac{Cf_{net}}{C_{capitalcost}} \left[ 1 - \frac{1}{(1+IRR)^M} \right] \quad (3.30)$$

Where M is the total operating year of the evaporative cooling device. The simple payback period is calculated as $SPP = \frac{C_{capitalcost}}{Cf_{net}}$ (3.31)

The payback period (PP) is calculated by taking into account of discount factor as:

$$PP = \frac{\ln\left[ \frac{Cf_{net}}{Cf_{net} - rC_{capitalcost}} \right]}{\ln(1+r)} \quad (3.32)$$

The parameters used in the economic analysis:, Discount factor (r) = 3% (Bellos et al.,2017), Device operating life (M) = 15 year, $COP_{eq}$ = 3 (4 star rated air-conditioning EER), $K_{o\&m}$ = 5% of the capital cost **(**Sohani et al.,2018**).**

### *3.2.5 Environmental analysis*

The production of energy from conventional resources causes harmful effects on the environment, such as ozone depletion, acid rain, and carbon emission. Electrical energy has used the device to operate a fan and pump. The electricity is produced from electric substations by consuming coal. The carbon emission for the production of electricity can be estimated by considering the carbon emission factor. The $CO_2$ release is calculated by (Caliskan et al., 2012),

$$P_{co_2} = \frac{f_{co_2} W_{Consumption} t_{Operation}}{10^6} \tag{3.33}$$

Where $P_{co2}$ is the ton of carbon produced in a year, the $f_{co2}$ is the carbon emission factor. This carbon emission factor depends upon the methods of electricity production and varies from country to country. The carbon emission factor for India 0.820 $kgCO_2/kWh$. The $W_{Consumptionn}$ is the power consumption during operating hours in kilowatt, and $t_{Operation}$ is the device running hour in h/year.

### *3.2.6 Sustainability analysis*

Sustainable development helps in the efficient utilization of the resources with taking care of the future also. Rosen et al. (2008) introduced a sustainability index for the efficient utilization of resources.

$$\text{Exergy ratio } (\Phi) = \frac{\dot{E}x_{out}}{\dot{E}x_{in}}, \text{ Sustainability index (SI)} = \frac{1}{1-\Phi} \tag{3.34}$$

Where $\dot{E}x_{out} = \dot{E}x_{supplyair\text{-}out} + \dot{E}x_{sa\text{-}out}$ and $\dot{E}x_{in} = \dot{E}x_{pa} + \dot{E}x_{w}$

### *3.2.7 Validation of simulation code*

The simulation code based on the equations mentioned above has been validated with the published experimental results of Riangvilaikul and Kumar (2010), as shown in Fig. 3.4. The configuration used is a counter flow regenerative mode similar to

configuration C in this paper. The specifications of the evaporative HMX used for validation are the gap of channels = 5 mm, length of channels = 1.2 m, the width of channels = 80 mm, and wall thickness = 0.5 mm. The operating conditions used are: inlet air velocity = 2.4 m/s, extraction ratio = 0.33, mass flow rate of water = 60 g/h and inlet temperature variation from 25 to 45 °C. The maximum percentage of deviation between the simulated result and the published experimental result is 2.16 %, which is acceptable. The physical model behind all the configurations is the same, and the only configuration effect needs to be investigated. Hence, this paper uses the above-validated model to investigate and compare the performance of all studied configurations.

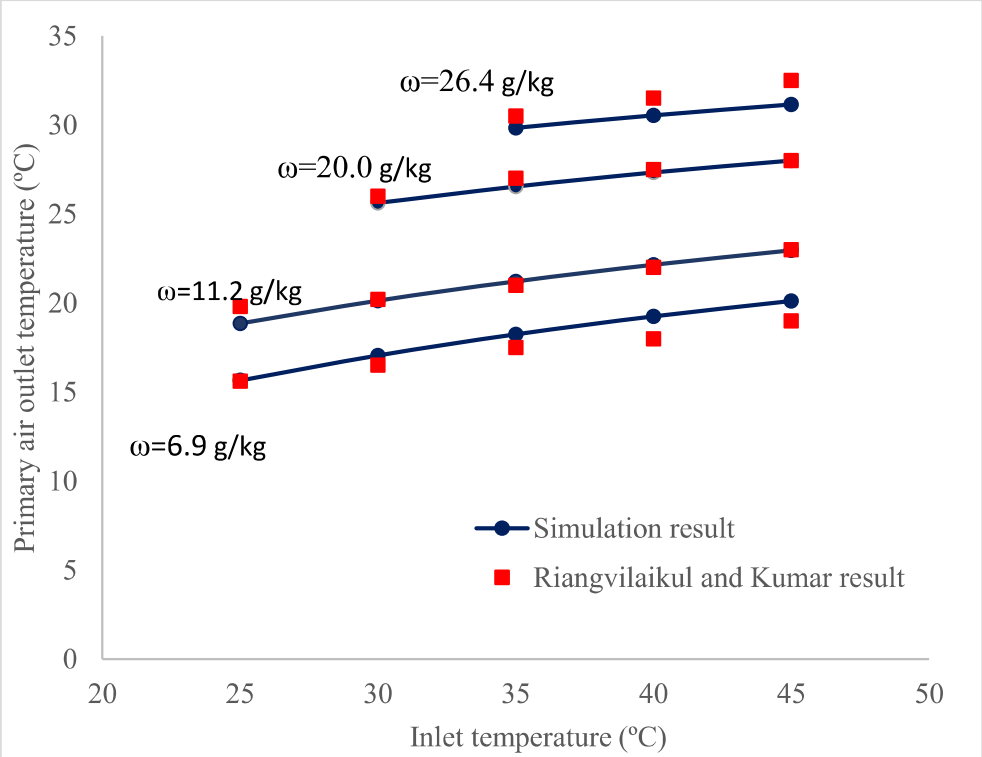


**Fig. 3.4** Validation of numerical simulation with the experimental result (Riangvilaikul and Kumar, 2010)

### 3.3 Results and discussion

The geometrical specification of the evaporative heat and mass exchanger is listed in Table 3.3. Unless otherwise specified, the mean operating conditions of the

regenerative evaporative cooler are assumed. Mean primary air inlet conditions are: dry-bulb temperature = 35 ºC, wet bulb temperature = 21.98 ºC, specific humidity = 11.2 g/kg of dry air and velocity = 2 m/s.

**Table 3.3**: Specification of HMX and mean operating parameters

| | |
|---|---|
| Length of the evaporative HMX | 0.5m |
| Width of the HMX | 0.5m |
| The total height of the HMX | 0.7 m |
| The gap between the primary air channel | 0.005 m |
| The gap between the secondary air channel | 0.005 m |
| The thickness of the plate separating two channels | 0.5 mm |
| The volumetric flow rate of water per channel | 5 L/h |
| The inlet temperature of the water | 17 ºC |
| Air extraction ratio | 0.3 |
| Total primary air flow rate ($V_{pa}$) | 0.35$m^3$/s |
| Total secondary air flow rate ($V_{sa}$) | 0.245$m^3$/s |
| Total supply air flow rate ($V_{out}$) | 0.105$m^3$/s |
| Pump efficiency | 60 % |
| Fan efficiency | 65% |

### *3.3.1 Energetic comparison*

The configurations of the regenerative evaporative cooler are compared on the basis of the dew point effectiveness, cooling capacity, and COP as listed in Table 3.4. The lowest supply air temperature is obtained for configuration A (20.63 ºC) and followed by configuration H (20.93 ºC). The lowest cooling capacity is obtained for configuration

C. The configurations A and H perform better in terms of effectiveness, cooling potential, and energy efficiency than the other ones.

**Table 3.4**: The energetic comparison of the different configurations

| Configurations | A | B | C | D | E | F | G | H |
|---|---|---|---|---|---|---|---|---|
| Dew point effectiveness (%) | 61.24 | 49.66 | 43.65 | 50.21 | 58.17 | 47.49 | 49.49 | 59.94 |
| Cooling capacity (W) | 3922 | 3180 | 2796 | 3215 | 3725 | 3042 | 3170 | 3839 |
| COP | 32.17 | 26.08 | 22.93 | 26.37 | 30.55 | 24.95 | 25.99 | 31.48 |

### *3.3.2 Exergetic comparison*

Fig. 3.5 shows the exergy distribution graph of configuration A when it is simulated at the mean operating conditions. The simulation is performed by taking ambient air (at ambient temperature) in the saturated conditions as the dead state. The primary air exergy is divided into two parts, mentioned in Fig. 3.5, as supply air inlet exergy and working air inlet exergy. The exergy destruction is 135.9 W, which accounts for 15.68% of the total input exergy. The supply air exergy contributes a maximum part of around 77.5% of the total input exergy. The rational selection of dead states makes the exergy of water input very small, while output exergy holds only 6.75% of the total input exergy. Table 3.5 shows the breakdown of the total flow exergy at the different thermodynamic states of the air in HMX. The chemical exergy of the inlet air remains constant from state 1 to 2 (Fig. 3.9) because heat exchange takes place at constant humidity conditions. The thermal exergy increases from point 1 to 2, while mechanical energy decreases due to flow resistance. The cooling effect is obtained due to the

conversion of chemical exergy in the wet channel (points 2 to 3). The thermal as well as chemical exergy both decreases in the wet channel of heat and mass exchange Table 3.6 shows the exergetic comparison of the different configurations at the mean operating conditions. The chemical exergy contains a major portion of the total flow exergy. The change of the chemical exergy is more significant, and mechanical exergy has the least contribution (due to low-pressure drop). The exergetics performance of configurations A and H is better than other configurations.

**Table 3.5**: The specific exergy of the air at a different point in regenerative HMX

| Air state | Primer air inlet | Supply air | Secondary air exit |
|---|---|---|---|
| Chemical exergy (J/kg) | $\Psi_{Chemical1}$=2.146 | $\Psi_{Chemical2}$ =2.146 | $\Psi_{Chemical3}$ =0.343 |
| Thermal exergy (J/kg) | $\Psi_{Thermal1}$ =0.0 | $\Psi_{Thermal2}$ =0.358 | $\Psi_{Thermal3}$ =0.100 |
| Mechanical exergy (J/kg) | $\Psi_{Mechanical1}$ =0.025 | $\Psi_{Mechanical2}$ =0.010 | $\Psi_{Mechanical3}$ =0.0 |

**Table 3.6**: The exergetic comparison of the different configurations

| Configurations | A | B | C | D | E | F | G | H |
|---|---|---|---|---|---|---|---|---|
| Exergy destruction(W) | 135.9 | 144.9 | 180.4 | 167.8 | 148.7 | 162.9 | 167.2 | 119.0 |
| Exergy efficiency (%) | 40.34 | 28.81 | 19.69 | 26.35 | 35.63 | 34.32 | 25.82 | 42.45 |
| Exergy ratio (%) | 84.32 | 83.28 | 79.18 | 80.63 | 82.83 | 81.20 | 80.70 | 86.27 |

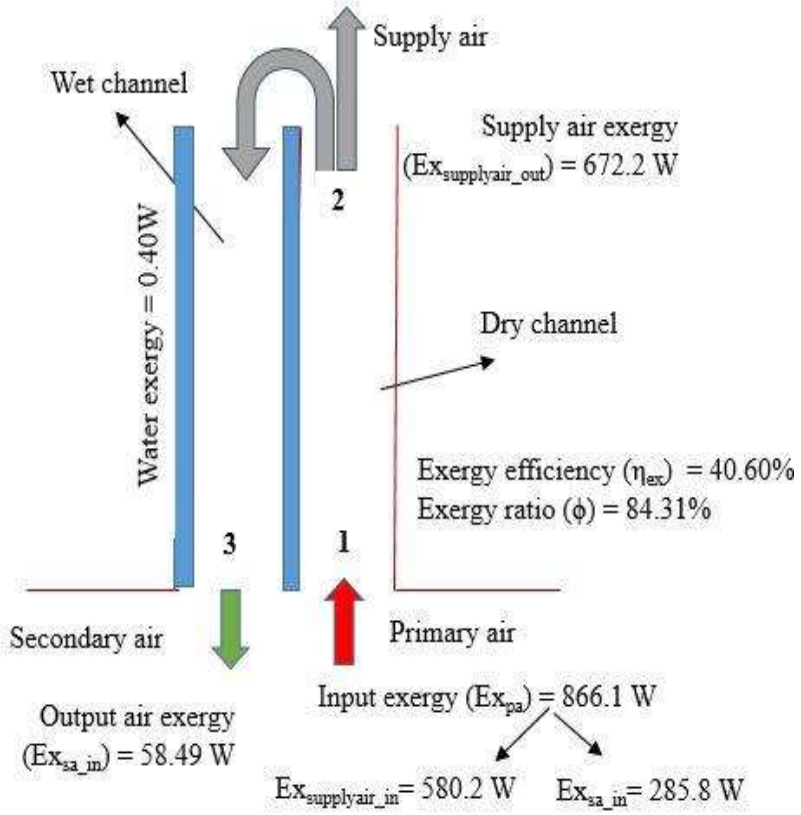


**Fig. 3.5** Exergy distribution graph of the configuration A (at the mean operating condition)

### *3.3.3 Economic comparison*

The capital cost of all the configurations remains the same, and it is around 457.7 USD by considering 30% of the manufacturer's profit. The running cost depends upon the pressure drop and water circuiting rate of the pump. Both parameters remain invariant for different configurations. The running cost of the HMX is calculated by taking the electricity price of 0.08 USD/kWh. The air filter pressure drop is added in the HMX and gives COP of the device around 35, which is further utilized in the economic and environmental analysis. The running cost of the HMX is around 12.99 USD, which holds true for low electricity tariff countries. The specific cost of the HMX at the mean operating condition for all HMX is specified in Table 3.7. The variation of parameters affects the running cost and specific cost significantly. The increase in the extraction ratio decreases the running cost of 13.35 USD to 10.99 USD, while increases in the channel

gap 0.3 mm to 0.7 mm decreases the running cost 13.56 USD to 12.43 USD. The increase in the volume flow rate of the primary air, increase running cost but decrease the total specific cost of the HMX. The net cash flow varied in the range of 71.48-114.7 USD, while the lowest for configuration C and highest for configuration A at the mean operating conditions. The NPV, IRR, SPP, and PP of all configurations are listed in Table 3.7. The NPV of all the configurations is positive and achieved the highest figure for configuration A. The highest IRR is 24%, which makes it a good and economically viable device. The average life of a cooler is 15- 20 years, while its SPP is in the range of 3.9 to 6.4 years. The PP of the best configuration is 4.3 years, so it's a good economic decision to have these eco-friendly devices.

**Table 3.7**: The specific total of the different configurations at mean conditions

| Configurations | A | B | C | D | E | F | G | H |
|---|---|---|---|---|---|---|---|---|
| Specific total cost (USD/kW) | 125.8 | 155.2 | 176.5 | 153.5 | 132.5 | 162.3 | 155.7 | 128.6 |
| NPV (USD) | 912.0 | 572.0 | 395.7 | 588.1 | 821.8 | 508.4 | 567.0 | 873.8 |
| IRR (%) | 24.08 | 17.07 | 13.00 | 17.42 | 22.27 | 15.70 | 16.97 | 23.32 |
| SPP (Years) | 3.9 | 5.3 | 6.4 | 5.2 | 4.2 | 5.6 | 5.3 | 4.1 |
| PP (Years) | 4.3 | 5.8 | 7.2 | 5.6 | 4.6 | 6.2 | 5.8 | 4.4 |

### *3.3.4 Environmental and Sustainability comparison*

The $CO_2$ emission is not fluctuating much with the use of the different configurations. The carbon emission factor for India is 0.82 $kgCO_2/kWh$. The $CO_2$ emission quantity depends significantly on the operating and geometrical parameters. This single heat and mass exchanger will produce 133.1 $kgCO_2$/year if operated for 180

days/year and eight working hours/day. The utilization of these evaporative HMX saves us from the production of large amounts of toxic carbon dioxide gases. If these devices are used instead of conventional mechanical vapor compression, a large amount of saving in CO2 emission will be achieved.

Sustainability represents ecologically balanced resource utilization. The sustainability index can be used as an instrument to measure the efficient conversion of natural resources to fulfill our needs by taking care of social responsibility. The sustainability index of all the configurations is at mean operating conditions are described in Table 3.8. The configuration H is the most sustainable configuration among all. All the configurations are closely sustainable enough. Since this evaporative HMX are energetically and energetically efficient, it obvious that it will save our resources.

**Table 3.8**: The sustainability index of the different configurations at mean conditions

| Configurations | A | B | C | D | E | F | G | H |
|---|---|---|---|---|---|---|---|---|
| Sustainability index | 6.377 | 5.981 | 4.800 | 5.164 | 5.826 | 5.319 | 5.182 | 7.282 |

### *3.3.5 Effect of water inlet conditions*

The flow rate of water is a very significant operating parameter in the analysis of the regenerative evaporative cooling exchangers. Only a few studies have been done on the effect of the water flow rate. In the literature, the very low water flow rate is taken for counter/parallel flow configurations while high mass flow rates for cross-flow configurations (Moshari et al., 2015). The dew point effectiveness of the device may increase or decrease with an increase in water mass flow rate depending upon the water inlet temperature. Figs. 3.5 and 3.6 show the variation of dew point effectiveness with the increase in water flow rate. The volumetric flow rate of water varies from 5 L/h to 50 L/h

in this study. The water evaporated to water supplied is approximately 1% for all the configurations at the volumetric water flow rate of 5 L/h. Hence, the fraction of evaporated water is very low, and the inlet temperature of the water is also an important parameter of the performance. Variation of cooling capacity and dew point effectiveness with water flow rate at different water inlet temperatures is shown in Figs. 3.6 and 3.7, respectively. The cooling capacity and dew point effectiveness both increase for water inlet temperature of 17 ºC and 19 ºC. The capacity directly related with the temperature drop. That's why cooling capacity increases with the increase in the flow rate. The performance of configuration A is higher than configuration H. The COP of the regenerative evaporative cooler decreases with the increase of the water flow rate for all the inlet temperature conditions, as shown in Fig. 3.8. The higher water flow rate improves energy performance marginally (for 17 and 19 ºC), while pump work increases, which results in the decrease in the coefficient of performance. The exergy efficiency of the regenerative evaporative cooler decreases for the 23 ºC water inlet temperature conditions for both A and H configurations, as shown in Fig. 3.9. Variation of dew point effectiveness with water inlet temperature is shown in Figs. 3.10 for parallel/counter-flow (configuration A) and cross-flow (configuration H), The temperature at which different lines cross each other depends upon the configuration. These temperature values are 24ºC, 25.5ºC, 21 ºC, and 26ºC for configurations A, B, C, and D, respectively. Approximately the same range of values is obtained for the cross-flow configurations. These crossing temperatures for configurations E, F, G, and H are 25 ºC, 23.2ºC, 26ºC, and 23.8ºC, respectively. If water inlet temperature is less than this crossing temperature, dew point effectiveness initially increases with the increase of the water flow rate and later becomes almost constant. In a practical situation, water inlet temperature lies in between the wet bulb and dew point temperatures of the atmospheric conditions. A higher (more than

water evaporated) water flow rate is required to maintain the whole surface uniformly wet and justify the unity wettability factor.

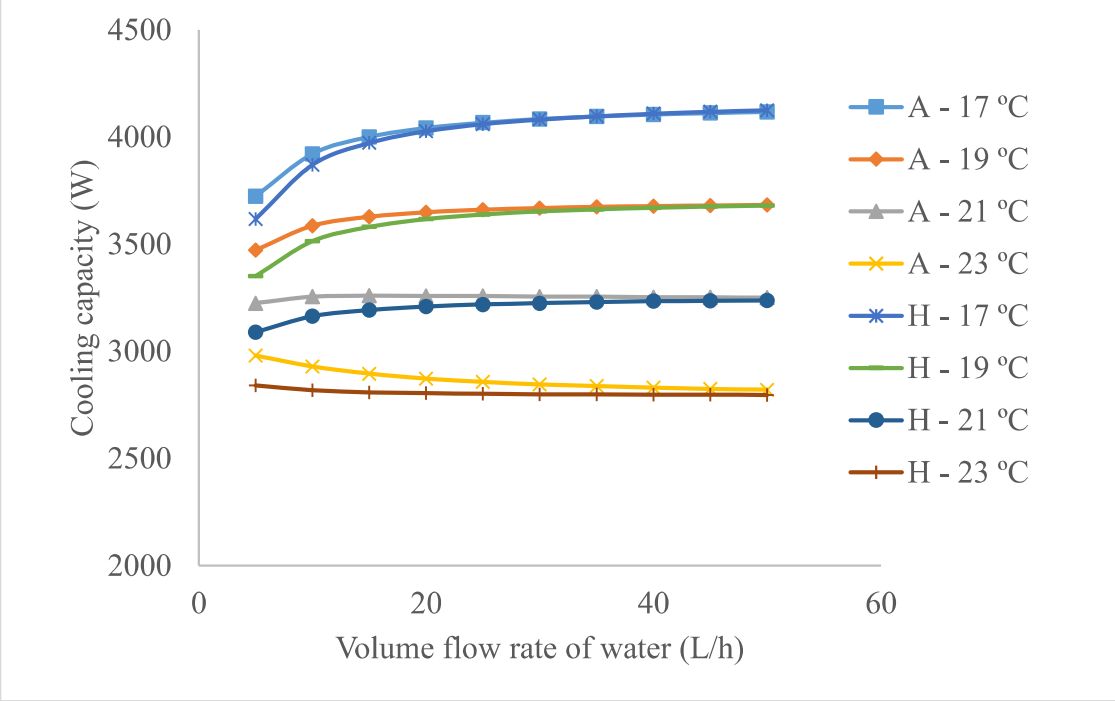


**Fig. 3.6**. Variation of cooling capacity with water flow rate for configuration A and H

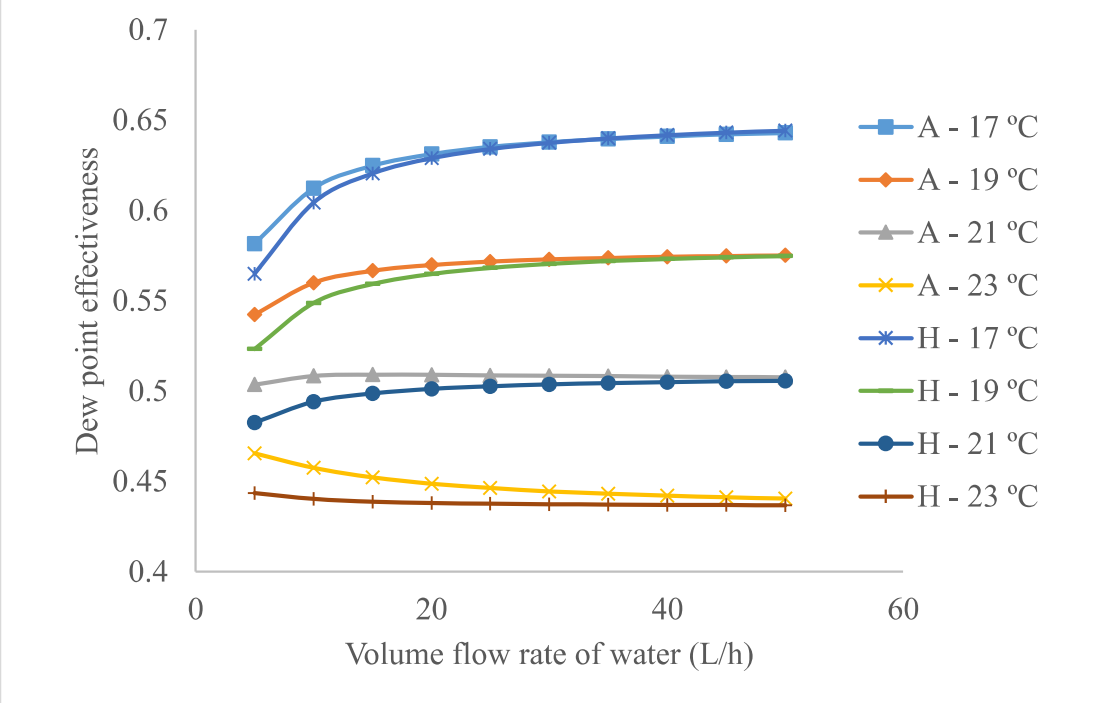


**Fig. 3.7**. Variation of dew point effectiveness with water flow rate for configuration A and H

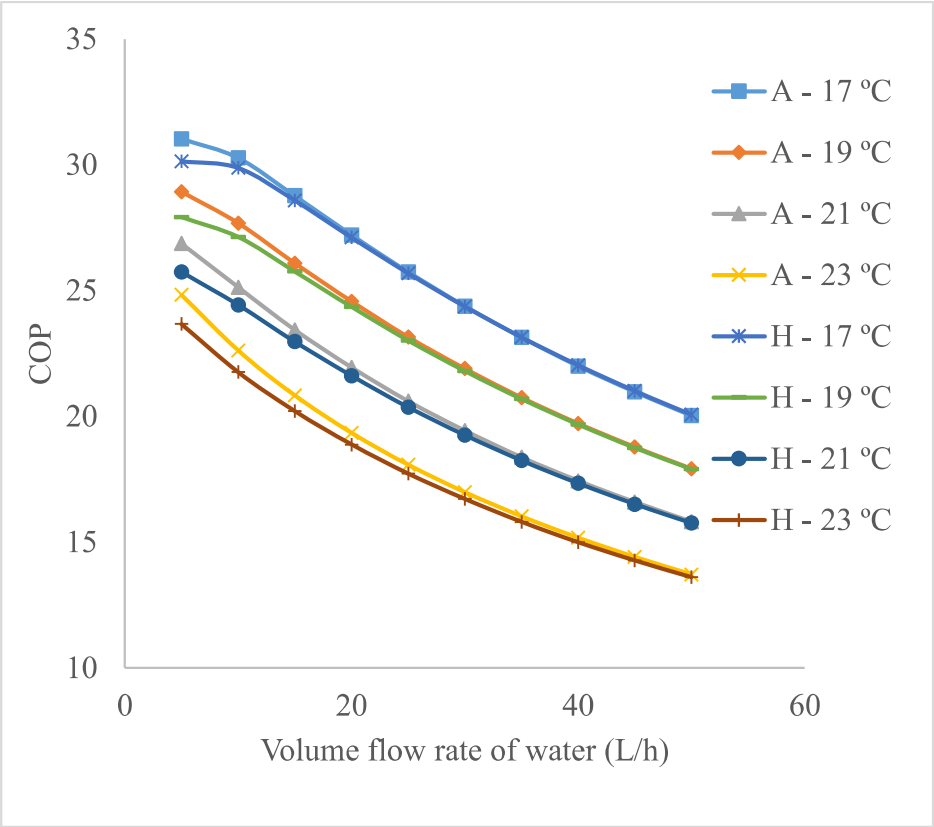


**Fig. 3.8**. Variation of COP with water flow rate for configuration A and H

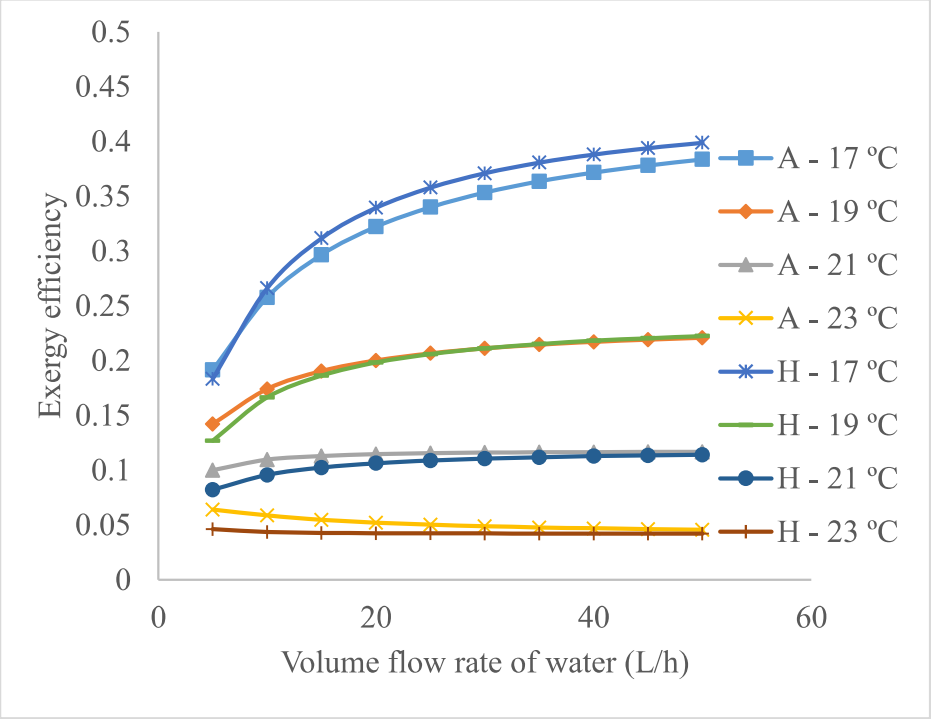


**Fig. 3.9** Variation of exergy efficiency with water flow rate for configuration A and H

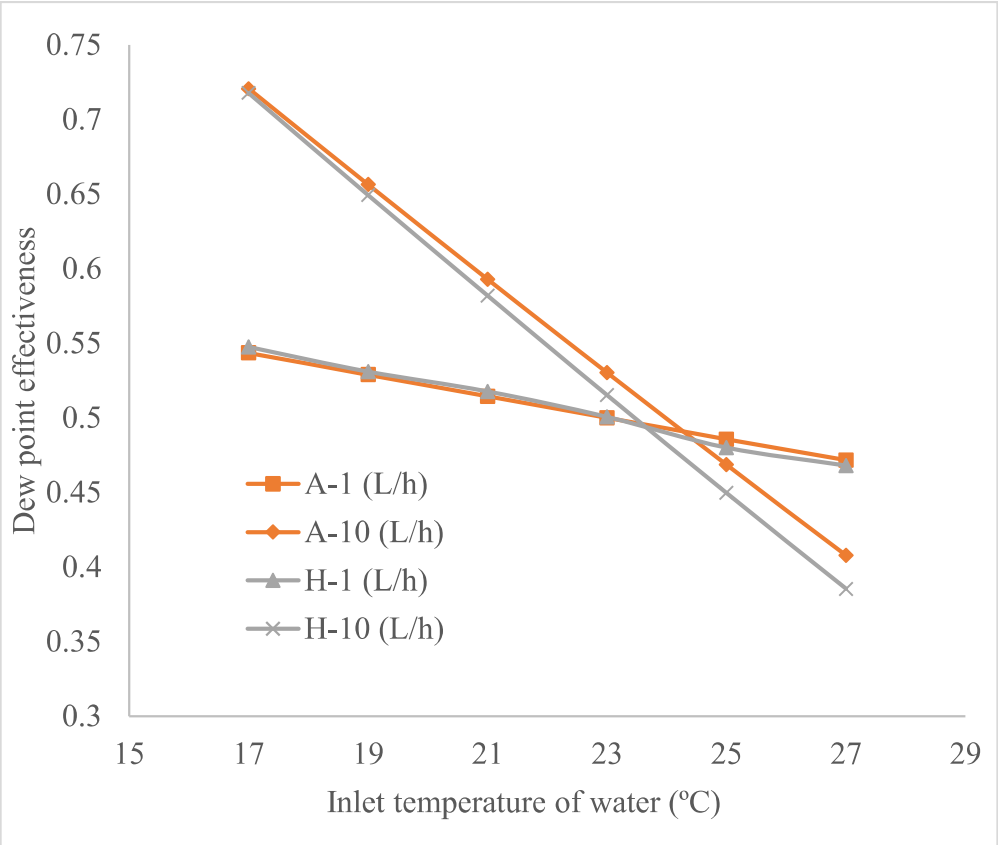


**Fig. 3.10** Variation of dew point effectiveness with water inlet temperature for configurations A to H

### *3.3.6 Effect of extraction ratio*

An increase in extraction ratio (secondary air to primary air mass flow rate ratio) improves the effectiveness of the exchanger for all configurations (Fig. 3.11). An increase in the secondary air mass flow rate for the same primary air works as an increased heat sink mass. This increased heat sink mass decreases outlet temperature, but the mass flow rate of supply air is reduced. The cooling capacity of the exchanger depends upon both the outlet temperature as well as the mass flow rate of the supply air. Fig. 3.12 shows exergy destruction and COP variation with the extraction ratio. The cooling capacity and COP of the regenerative evaporative cooler decrease with an increase in the extracted air. The reduced mass flow rate of supply air affects more as compared to the increased

temperature drop with the increase in the extraction ratio. The difference between the cooling capacities of all configurations is higher at the lower extraction ratio. The low value of extraction ratio produces a higher supply air temperature, and this temperature varies significantly for different counter and cross-flow configurations. At the higher extraction ratio, the difference in cooling capacity and COP is less for A and H configurations of the regenerative evaporative cooler. The Exergy destruction of all HMX increases with the increase in the extraction ratio. An increase in the extraction ratio increases the mass flow rate in the wet channel. The more mass for heat and mass exchange causes more exergy destruction in the system. The exergy destruction increases for configurations (A and H) of HMX. The increase in exergy destruction decreases the exergy efficacy of all configurations, as shown in Fig. 3.13. The specific total cost increases due to decreases in COP. The exergy efficiency is maximum at 0.3 extraction ratio, which shows that at this condition, the maximum work potential of the wet channel air is extracted. The exergy efficiency difference between the different configurations decreases as the extractions ratio increases. The sustainability index also decreases as the extraction ratio increases from 0.3 to 0.7, as shown in Fig. 3.14. The sustainability index depends upon the exergy ratio (output exergy/input exergy). The higher extraction ratio decreases the exergy ratio, which makes the HMX less sustainable. The sustainability index gap between the different configurations decreases with the increase of the wet channel air mass flow rate (Fig. 3.14). The carbon emission increases due to decreases in an energetic performance. The increase in the extraction ratio from 0.3 to 0.7 increases the $CO_2$ emission from 66.4 $kgCO_2$/year to 113.7 $kgCO_2$/year.

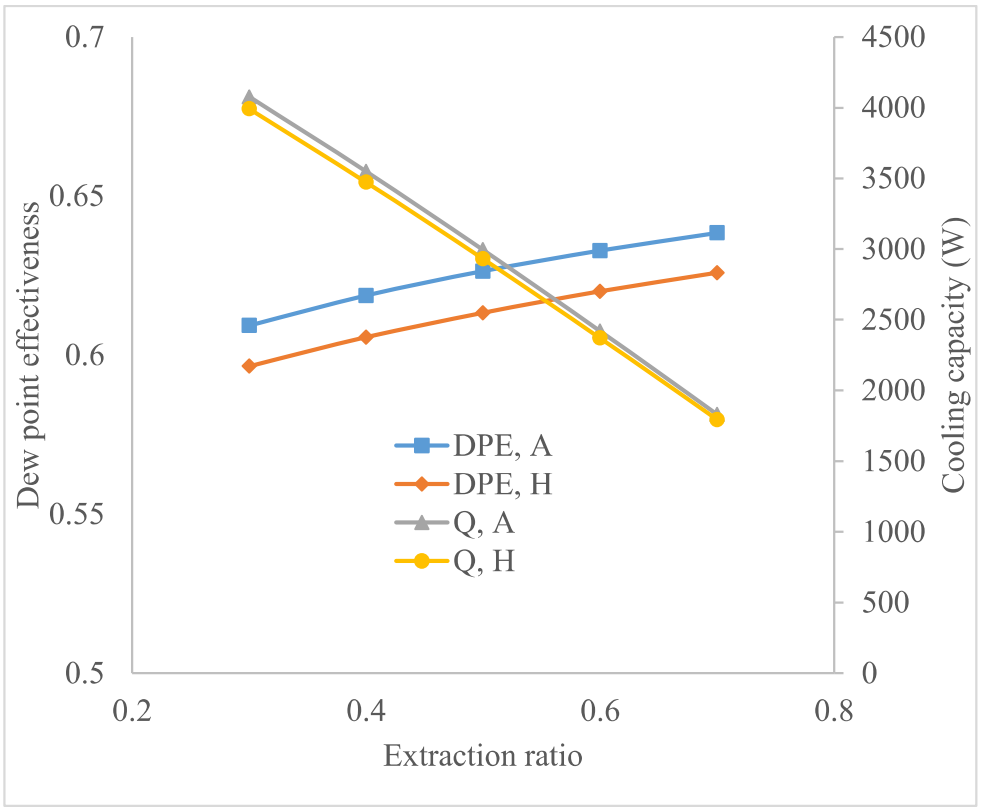


**Fig. 3.11** Variation of dew point effectiveness and cooling capacity with an extraction ratio

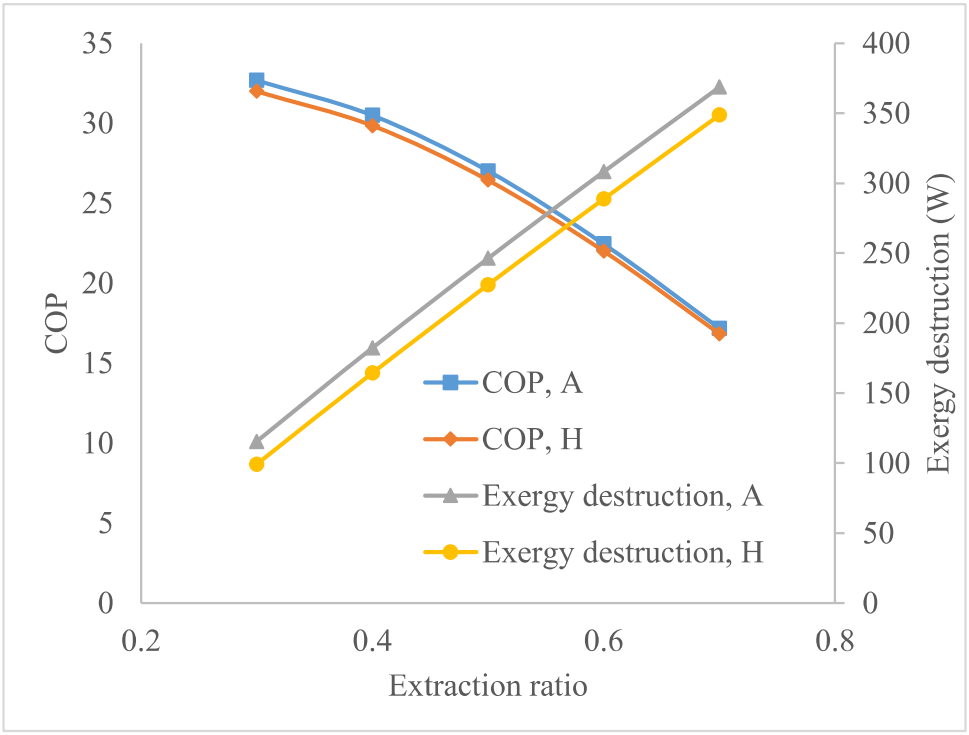


**Fig. 3.12** Variation of COP and exergy destruction with an extraction ratio

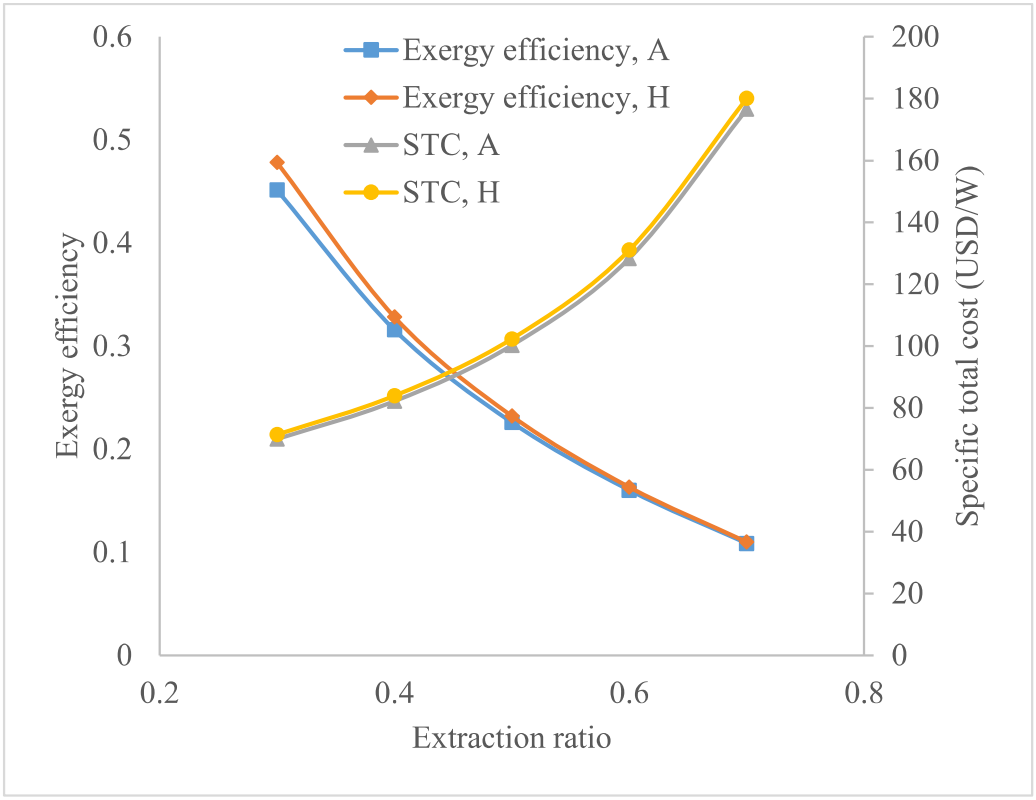


**Fig. 3.13** Variation of exergy efficiency and specific total cost with an extraction ratio

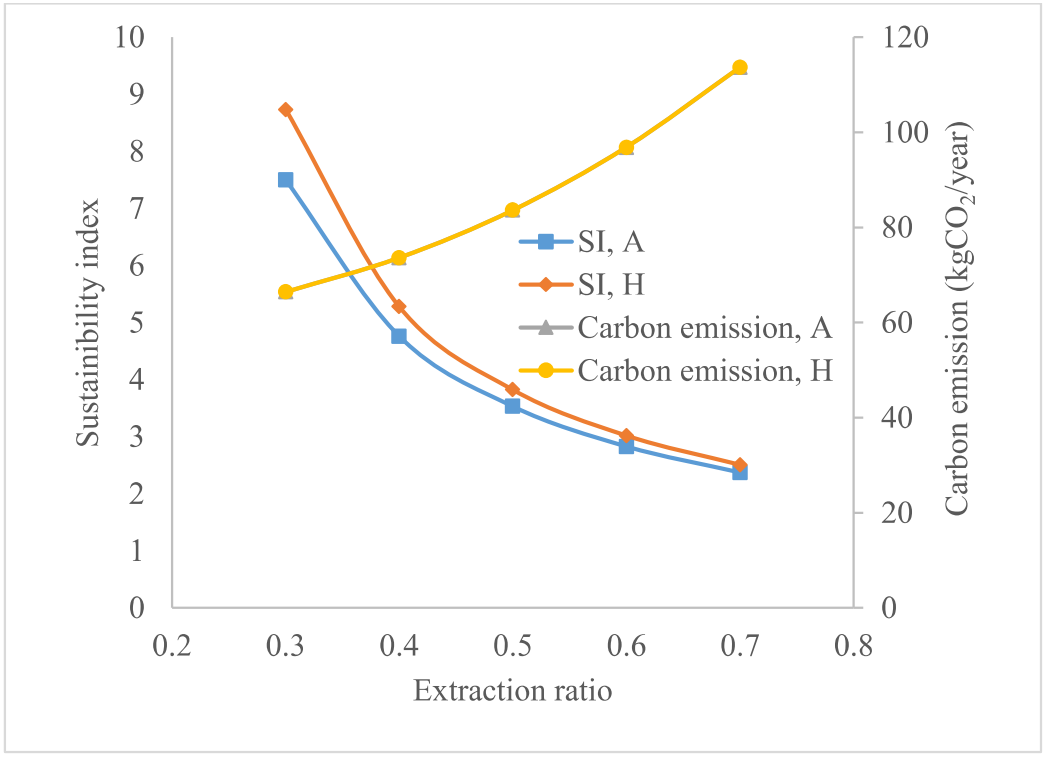


**Fig. 3.14** Variation of sustainability index and carbon emission with an extraction ratio

### *3.3.7 Effect of channel gap*

The cooling effect of the regenerative evaporative cooler improves with the decrease in gaps of the primary and secondary air channels. As shown in Fig. 3.15, the dew point effectiveness of all configurations improves with the decrease in the gap of the channels. At a lower channel gap, the cooling effect of configuration A is highest. The heat transfer coefficient of air increases with the reduction of the channel gap, which yields more cooling capacity, as shown in. This is also due to the fact that the total number of channels increases with a decrease in channel gap for a fixed outer dimension of the regenerative evaporative cooler, and hence total heat transfer area increases. The pressure drop also increases with the reduction in channel gap, and hence, more fan power is required to blow the air in both channels. The lower gap or smaller spacing of the channel provides more cooled air, but the required fan power to the device also increases. As shown in Fig. 3.16, COP of the heat and mass exchanger decreases with the increase of channel gap spacing. So there must be a compromise between the cooling temperature and COP of the device for all the configurations. The channel gap is optimized to deliver the supply air temperature in the thermal comfort zone and to have the maximum cooling capacity. The effect of the channel gap is not configuration specific, but it affects the performance of all configurations equally. The exergy destruction of all HMX increases with increases in the channel gap. The supply air temperature and pressure drop in the channels get affected mostly by the variation of the channel gap. The increase in the channel gap reduces the cooling effectiveness of the device. The available energy of the wet channel air is not completely utilized in the dry channel cooling effect. The increased channel gap increases the exergy destruction and affects the cooling effect of the regenerative evaporative HMX. The exergy destruction is lowest for configuration H, while the exergy destruction gap between the different configurations reduces at a wider

channel gap. The exergy efficiency of all the configurations decreases with the increases of the channel gap, as shown in Fig. 3.17. The specific total cost increases at the higher channel gap while it remains constant until 4 mm gap. Configuration H shows the highest exergy efficiency among all configurations. The sustainability index graph also follows the exergy efficiency trends (Fig. 3.18). The difference between the sustainability index values for both configurations is significant at a smaller channel gap. The carbon emission was reduced for HMX due to decreases in energy consumption (fan power) at a high channel gap. The increase in the channel gap decreases environmental degradation. The $CO_2$ emission decreases from 133.3 $kgCO_2$/year to 48.9 $kgCO_2$/year when the channel gap increases from 3 mm to 7 mm.

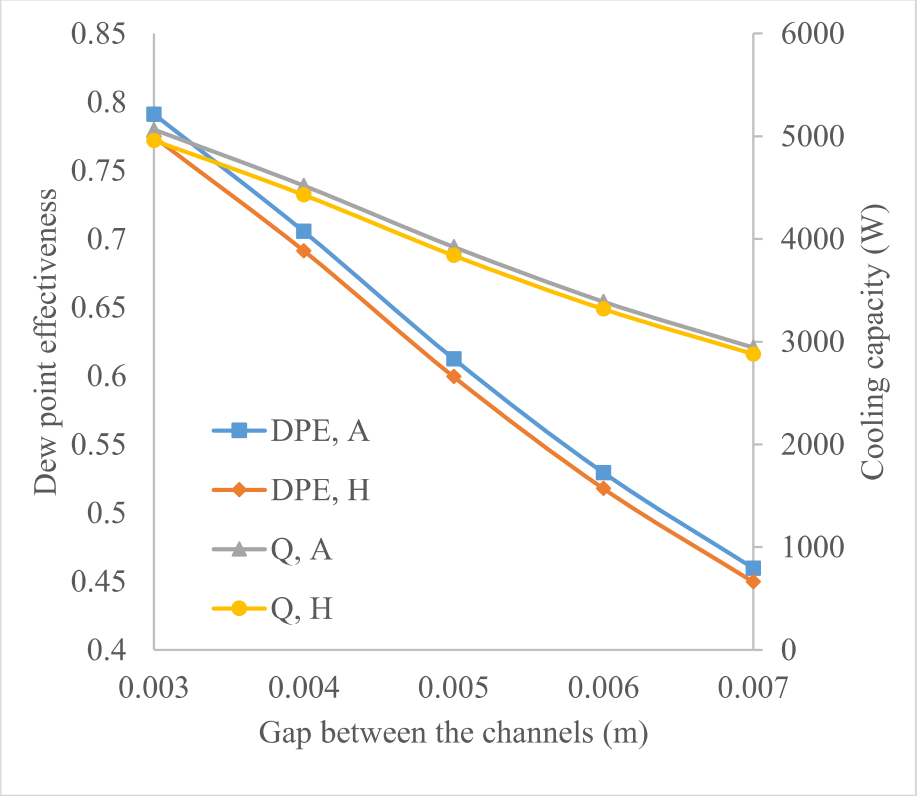


**Fig. 3.15** Variation of dew point effectiveness and cooling capacity with channel gap

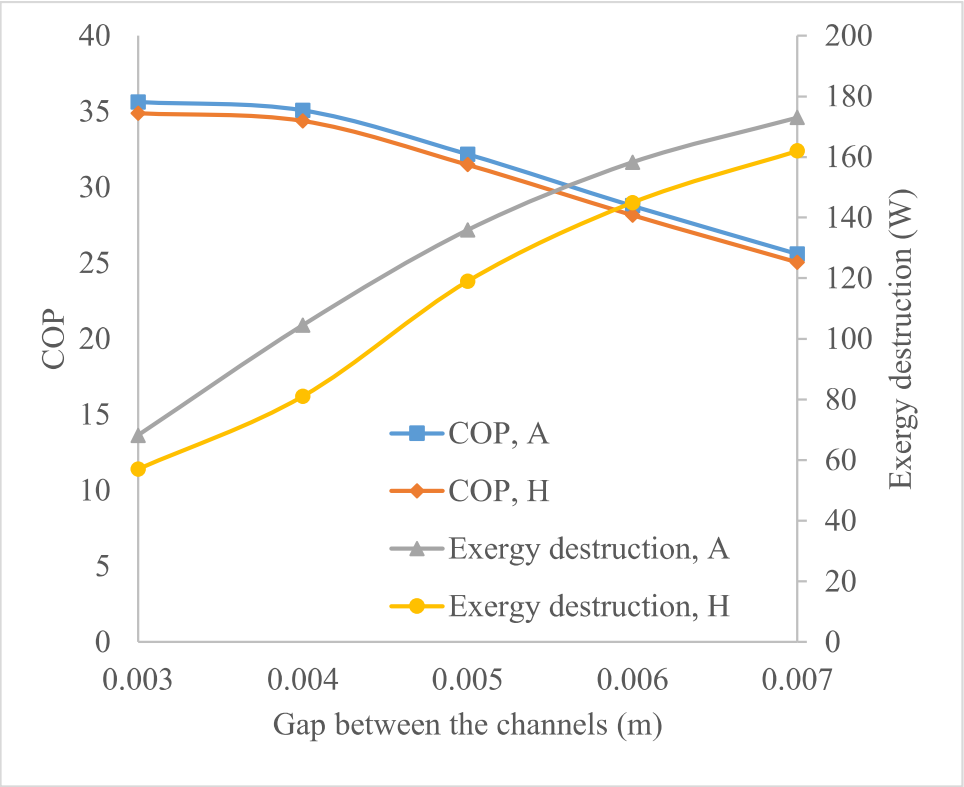


**Fig. 3.16** Variation of COP and exergy destruction with channel gap

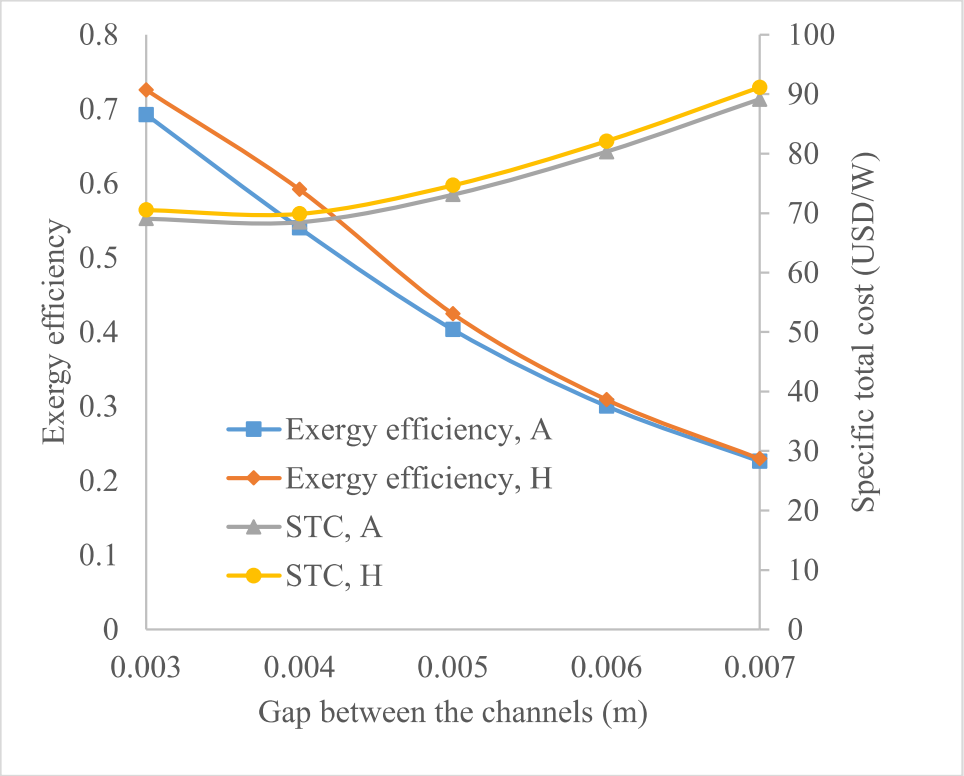


**Fig. 3.17** Variation of exergy efficiency and specific total cost with channel gap

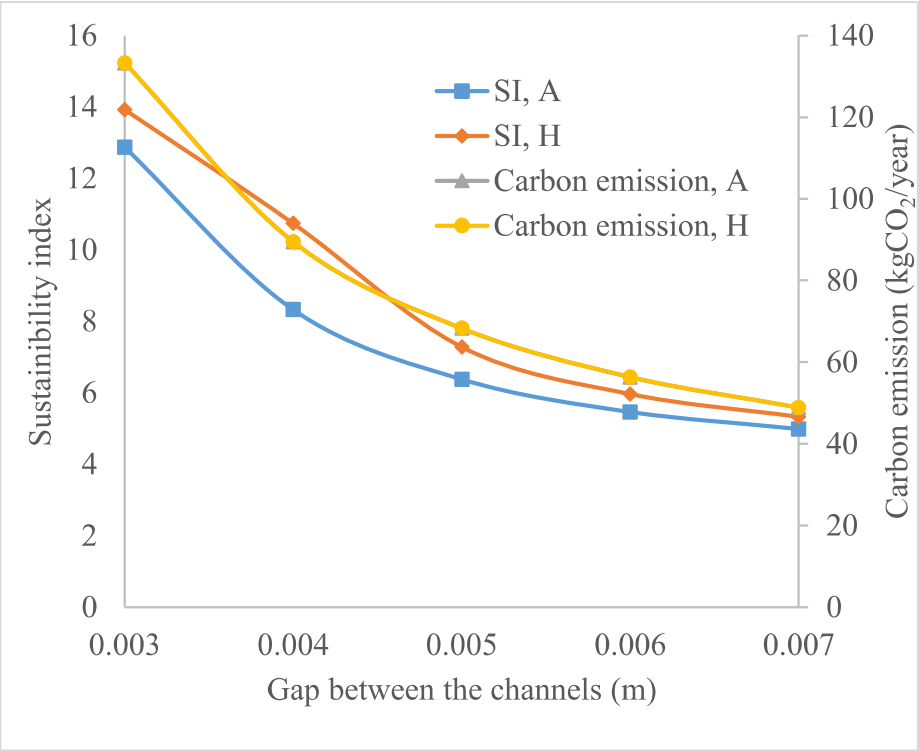


**Fig. 3.18** Variation of sustainability index and carbon emission with channel gap

### *3.3.8 Effect of inlet air flow rate*

As shown in Figs. 3.19 and 3.20, the increased flow rate of primary air reduces the dew point effectiveness and COP of the regenerative evaporative cooler. The change in dew point effectiveness and COP is rapid for the flow rate up to 0.3 $m^3/s$ and then gradually for all configurations. The cooling effect reduces because the increased flow rate reduces the interaction time of heat and mass exchanges. The cooling capacity of configurations increases with an increase in flow rate (or primary air velocity). The cooling capacity of the regenerative evaporative cooler improves because the increased mass of supply air enhances heat transfer. At a lower air inlet velocity, the difference in the cooling capacity for the configurations is less as compared to the same at higher velocity. The supply air temperature increases at a higher velocity, but it is dominated by a higher mass flow rate in terms of gain in the cooling capacity of the evaporative cooler. The difference in the cooling capacity for the configurations is in the closer range at low

velocity while it is significantly large at higher primary air velocity. It may be noted that as the water velocity is negligible as compared to air velocity, the effect of the flow rate of air on performance is more predominant. The increase in the volume flow rate of air increases the exergy destruction of the HMX, as shown in Fig. 3.21. The increased velocity of the air in the channel makes exergy destruction more profound. The faster the process of heat and mass transfer and the larger difference makes it more irreversible. The exergy destruction for all the configurations almost linearly increases with the increase of the volume flow rate. The increased exergy destruction with the increase in volume flow rate decreases the exergy efficiency of the heat and mass exchanger, as shown in Fig. 3.21. The specific total cost also decreases with an increased volume flow rate for both configurations. The exergy efficiency performance of the configurations H is the highest among all configurations. The exergy efficiency of all configurations decreases rapidly unto 0.35 $m^3/s$. The sustainability index of all the configurations decreases with the increase in the volume flow rate, as shown in Fig. 3.22. The configuration H was found to be the most sustainable configuration among all. The effect of the volume flow rate is not configuration specific, but it affects the performance of all configurations equally. The carbon emission increases with the increases in the volume flow rate of air. The increases in the volume flow rate increase the $CO_2$ emission drastically. The increased volume flow rate increases cooling capacity, but it decreases COP, which leads to a bad environmental effect. The co2 emission increases from 25.4 $kgCO_2$/year to 160.5 $kgCO_2$/year when the volume flow rate increases from 0.175$m^3/s$ to 0.525 $m^3/s$. The more volume of air in the channels requires more fan power to operate the device. It's must be ensured that supplying air temperature is in the thermal comfort zone, and there may be a compromise at this cost.

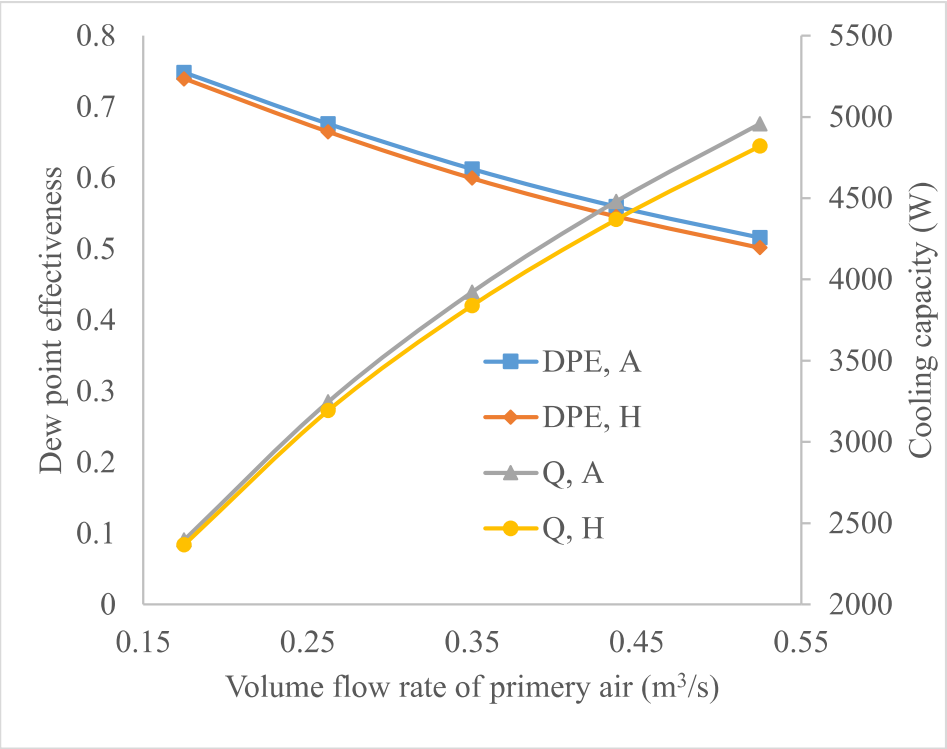


**Fig. 3.19** Variation of dew point effectiveness and cooling capacity with primary air flow rate

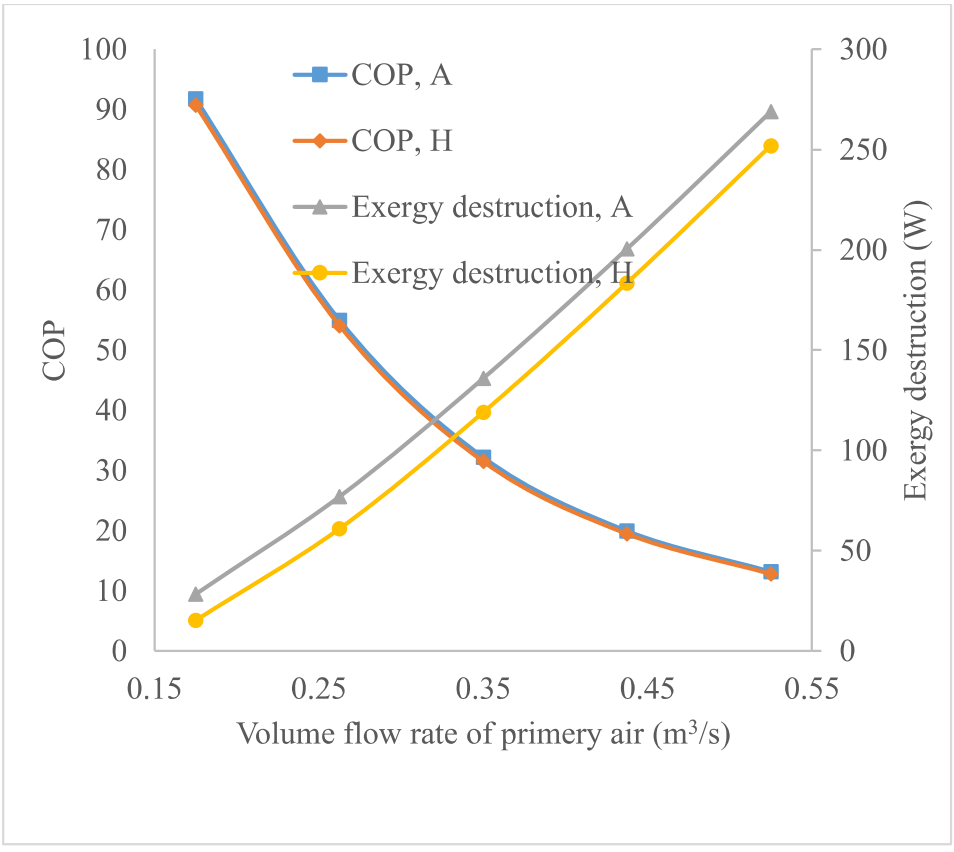


**Fig. 3.20** Variation of COP and exergy destruction with primary air flow rate

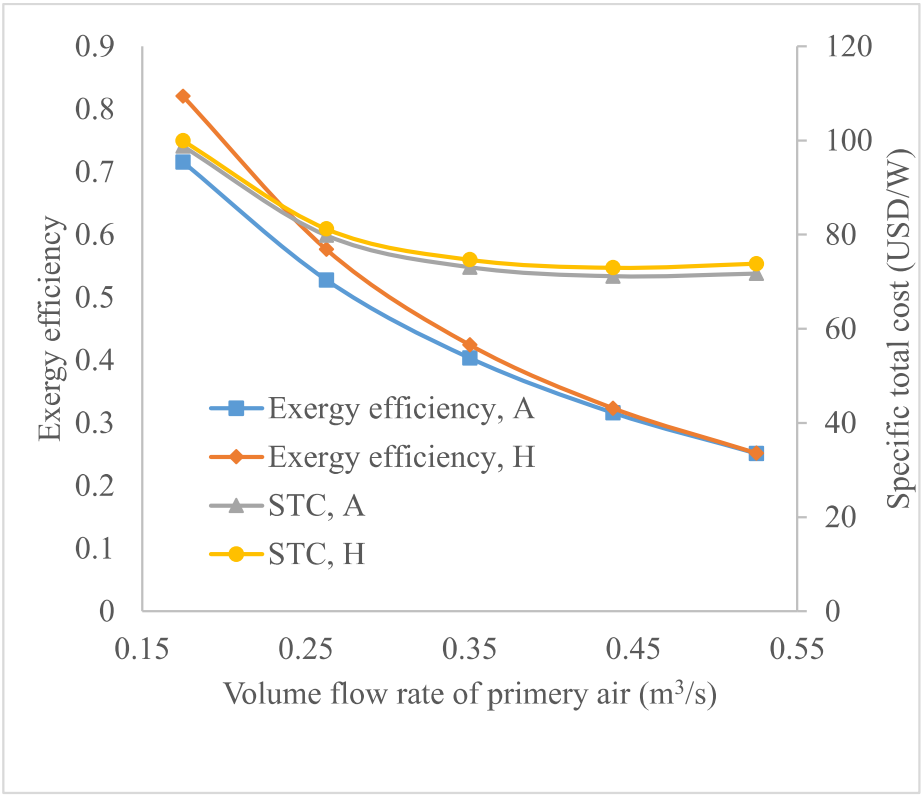


**Fig. 3.21** Variation of exergy efficiency and specific total cost with the primary air flow rate

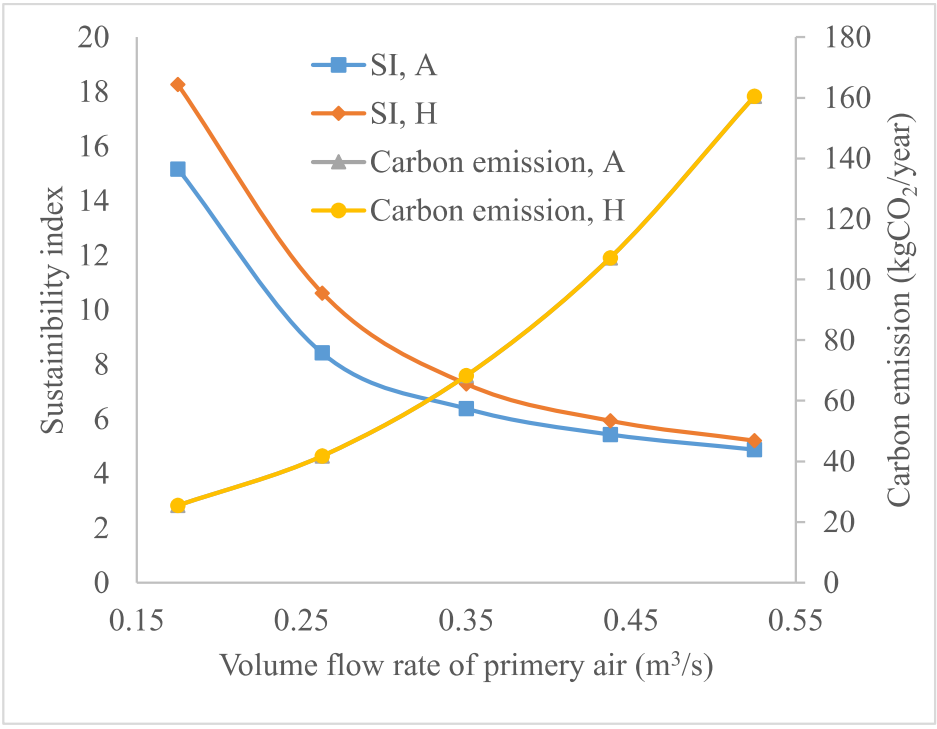


**Fig. 3.22** Variation of sustainability index and carbon emission with the primary air flow rate

### *3.3.9 Effect of inlet wet-bulb temperature*

The performance of various regenerative evaporative cooler topologies is simulated for a fixed inlet temperature of 35 ºC and varying the primary air inlet wet bulb temperature (20 ºC to 30 ºC). The outlet temperature of all configurations increases with the increase of the wet-bulb temperature. The increased wet-bulb temperature reduces the scope of more water evaporation which results in a lower temperature drop. However, the maximum possible temperature drop also decreases, and as a combined effect, the dew point effectiveness of all configurations increases with the increase of the wet-bulb temperature (Fig. 3.23). Here, the performance of configuration A is better than that of other configurations. The performance of the evaporative cooler in this case, too, is not configuration specific. The difference in the effectiveness of all configurations is not significant at higher wet bulb temperatures. The increase in wet bulb temperature reduces the temperature drop and hence the supply air temperature, which results in lower cooling capacity for all configurations. The cooling capacity of configurations A is highest among all eight configurations of evaporative cooler. The pressure drop of air inside the channels and hence the fan power of regenerative evaporative cooler remains the same, and pump power is very less compared to fan power. Hence, the COP of the device also yields a similar trend with the inlet air wet-bulb temperature for all configurations (Fig. 3.24). The exergy destruction decreases with the increase in the wet-bulb temperature. The sustainability index increases marginally (Fig. 3.25) while specific total cost increases significantly at higher inlet wet bulb temperature. The diminished cooling capacity contributes significantly to this specific total cost reduction.

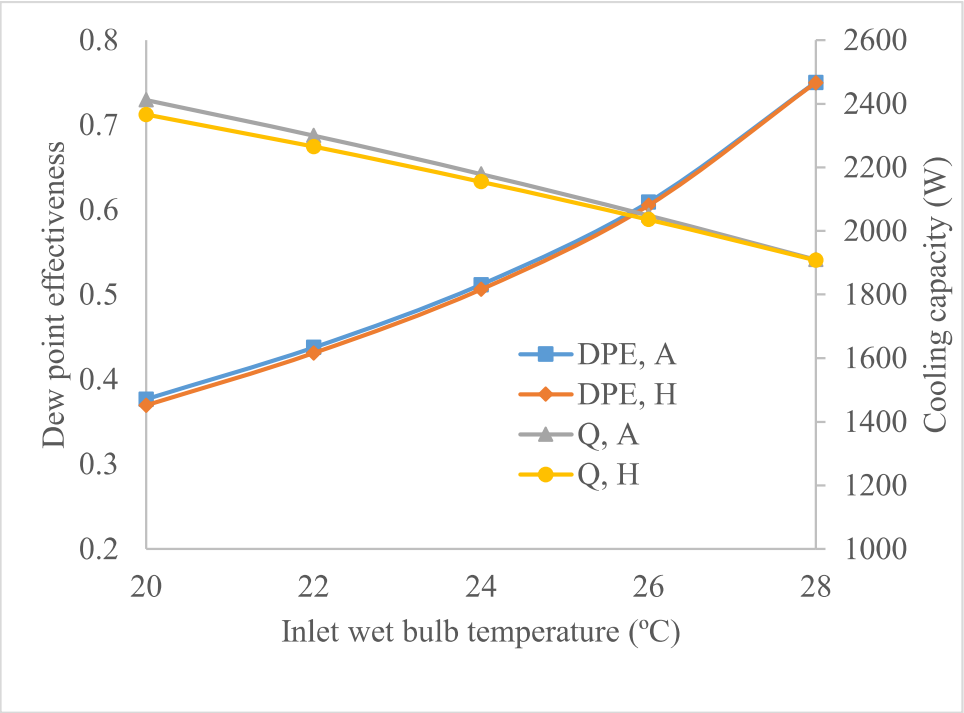


**Fig. 3.23** Variation of dew point effectiveness and cooling capacity with inlet air wet bulb temperature

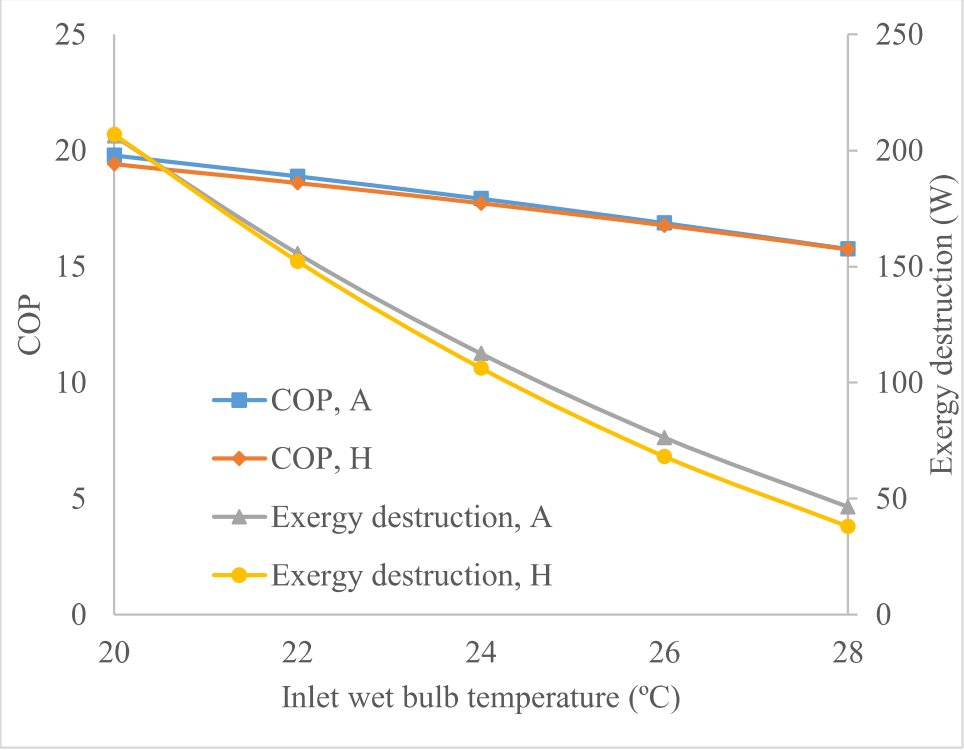


**Fig. 3.24** Variation of COP and exergy destruction with inlet air wet bulb temperature

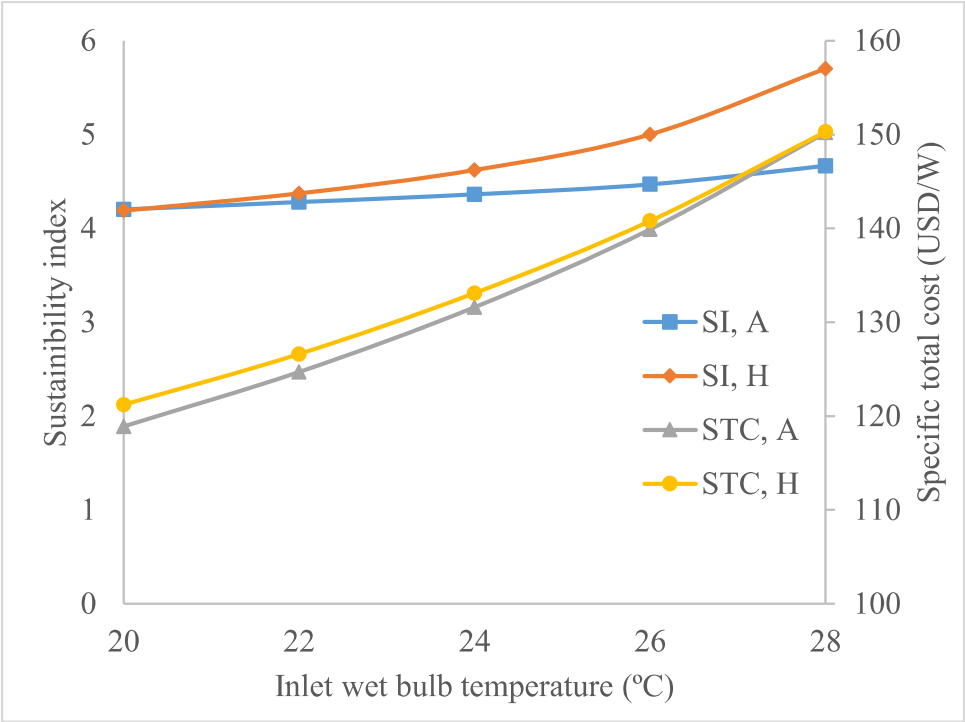


**Fig. 3.25** Variation of sustainability index and specific total cost with inlet air wet bulb temperature

### 3.4. Important findings

This work numerically investigates the performance of all possible configurations of the regenerative indirect evaporative heat and mass exchanger, which includes four configurations of parallel/counter flow while four configurations of the cross-flow. All eight configurations are compared based on cooling capacity, dew point effectiveness, COP, energetic, economic, and environmental parameters. The effects of various operating and design parameters are studied. The main conclusions are as follows:

- Both the water inlet temperature and mass flow rate affect the performance of the evaporative heat and mass exchanger significantly. Furthermore, the effect of temperature is more significant at a higher flow rate.
- There is a crossing temperature that depends on the configurations of parallel/counter and cross-flow heat and mass exchangers.

- If the water inlet temperature is less than the crossing temperature, dew point effectiveness improves with an increase in the mass flow rate of water and vice versa for all configurations.
- An increase in the extraction ratio improves the dew point effectiveness but reduces the cooling capacity of the indirect evaporative exchanger for all the configurations.
- The decrease in the gap of the air-flow channels improves the cooling effect of the evaporative exchangers for all the configurations.
- Increased velocity of primary air (increased mass flow rate in channels) reduces the dew point effectiveness of the evaporative exchanger for all the configurations.
- There is the highest contribution of chemical exergy change in the evaporative cooling process of the regenerative heat and mass exchanger.
- The increase in the extraction ratio increases the exergy destruction, which leads to the loss of exergy efficiency of regenerative HMX.
- The smaller channel gap makes the regenerative HMX exegetically efficient and environmentally sustainable.
- The increased volume flow rate (increased velocity of primary air) increases the exergy destruction and lowers the sustainability index of regenerative HMX.
- The carbon dioxide emission is almost constant for all configurations, but it varies significantly with varying operating and geometric parameters.
- Within studied configurations of regenerative HMX, A and H are best in terms of lower specific total cost and higher sustainability index